



# Response of particle number concentrations to the clean air action plan: lessons from the first long-term aerosol measurements in a typical urban valley in western China

Suping Zhao<sup>1,2,3,4</sup>, Ye Yu<sup>1,2,3</sup>, Jianglin Li<sup>1,2,3</sup>, Daiying Yin<sup>5,6</sup>, Shaofeng Qi<sup>1,6</sup>, and Dahe Qin<sup>4</sup>

<sup>1</sup>Key Laboratory of Land Surface Process and Climate Change in Cold and Arid Regions, Northwest Institute of Eco-Environment and Resources, Chinese Academy of Sciences, Lanzhou 730000, China

<sup>2</sup>Pingliang Land Surface Process & Severe Weather Research Station, Pingliang, 744015, China

<sup>3</sup>Gansu Land Surface Process & Severe Weather Observation and Research Station, Pingliang, 744015, China

<sup>4</sup>State Key Laboratory of Cryospheric Science, Northwest Institute of Eco-Environment and Resources, Chinese Academy of Sciences, Lanzhou 730000, China

<sup>5</sup>Key Laboratory of Desert and Desertification, Northwest Institute of Eco-Environment and Resources, Chinese Academy of Sciences, Lanzhou 730000, China

<sup>6</sup>University of Chinese Academy of Sciences, Beijing 100049, China

**Correspondence:** Suping Zhao (zhaosp@lzb.ac.cn)

Received: 25 May 2021 – Discussion started: 15 July 2021

Revised: 5 September 2021 – Accepted: 14 September 2021 – Published: 8 October 2021

**Abstract.** The strictest ever clean air action (CAA) plan has been implemented by the Chinese government since 2013 to alleviate the severe haze pollution. The  $\text{PM}_{2.5}$  mass concentration was found to largely be reduced in response to emission mitigation policies, but the response of particle number concentrations (PNCs) to CAA was less evaluated in the previous studies, which may be significantly different from  $\text{PM}_{2.5}$  mass due to newly formed particle impacts. In this work, the first in situ observation of particle number size distributions (PNSDs) during 2012–2019 in urban Lanzhou was used to analyze long-term PNC variations and CAA impacts. The average number of particles in nucleation ( $N_{13-25}$ , particle number in the size range of 13–25 nm), Aitken ( $N_{25-100}$ , particle number in the size range of 25–100 nm) and accumulation ( $N_{100-800}$ , particle number in the size range of 100–800 nm) modes were respectively 2514.0, 10 768.7 and  $3258.4 \text{ cm}^{-3}$ , and  $N_{25-100}$  accounted for about 65.1 % of total PNCs during the campaign. The  $k$ -means clustering technique was used to classify the hourly mean PNSDs into six clusters, and each cluster corresponded to a specific source and influencing factor. The polluted clusters governed the winter PNCs before 2016, and their occurrence was less and less frequent after 2016, which was largely dominated by re-

duction in primary emissions. However, the contribution of new particle formation (NPF) events to summer  $N_{13-25}$  decreased from 50 % to about 10 % during 2013 to 2015 and then increased to reach around 60 % in 2019. The trends of size-resolved PNCs for each cluster were quantified by Theil–Sen regression. The size-segregated PNCs exhibited downward trends for all clusters during 2012–2015, especially in spring. The annual relative slopes of spring PNCs varied from  $-54.7 \%$  to  $-17.2 \%$ ,  $-42.6 \%$  to  $-14.1 \%$ , and  $-40.7 \%$  to  $-17.5 \%$  per year for 13–25, 25–100, and 100–800 nm size ranges, and the reduction in the polluted clusters was much larger than NPF clusters. The ultrafine particle number was increased, and the amplitude was much greater during 2016–2019. The annual relative slopes of  $N_{13-25}$  varied between 8.0 % in fall and 135.5 % in spring for the NPF cluster. In response to CAA, the increased daytime net radiation, higher ambient temperature and lower relative humidity at noon for NPF events also could partly explain the higher  $N_{13-25}$  induced by the more frequent nucleation events after 2016, especially in spring. The air masses were mainly from the adjacent regions of urban Lanzhou and less affected by long-range transport for NPF events, and thus the particles were not easily grown by coagulation during transport pro-

cesses, which was helpful for the occurrence of NPF events. Therefore, some effective measures to cooperatively control particle number concentration and mass should be taken for the Chinese megacities.

## 1 Introduction

China has been experiencing large-scale and long-lasting winter haze pollution due to fast-growing economy and urbanization in past decades. The high concentration of aerosols perturbs the radiative balance of the atmosphere and surface by directly scattering and absorbing solar radiation or by indirectly altering cloud optical properties and cloud lifetime serving as condensation nuclei and ice nuclei (Andreae and Rosenfeld, 2008; Gao et al., 2015; Li et al., 2017). The adverse effect of deteriorated air quality on public health is of the greatest concern in China (Hu et al., 2017; Lelieveld et al., 2015). The present air quality standards consider particle mass instead of number concentration (WHO, 2000). However, compared to the larger aerosol particles, the ultrafine particles (UFPs, diameter < 100 nm) scarcely contribute to aerosol mass, while they share the largest number fraction in urban areas (Hussein et al., 2004; Wehner et al., 2004). The toxicity of UFPs is enhanced by the large surface area due to high number concentrations, and they can penetrate deep into the lungs, ending up in the blood circulation (Oberdörster et al., 2005; Schmid and Stoeger, 2016).

Aerosols' ability to efficiently scatter or absorb light depends not only on their chemical composition but on their sizes as well (Asmi et al., 2013). Liu et al. (2020) indicated that coating plays an important role in light absorption. The amplification of black carbon absorption by the coating increased from 1.21 to 1.75 with increasing aerodynamic diameter ( $D_{ac}$ ) due to the thicker coating of BC-containing particles with a larger  $D_{ac}$ . Their study highlights the strong dependence of the microphysical and optical properties of BC on size. The more recent study of Zhao et al. (2021) found that interdecadal AOD had a negative trend from 2009 to 2018, which may be related to the variation in particle size distribution. Some aerosol monitoring networks were established around the world for long-term measurements of climate-relevant aerosol properties, such as Geophysical Monitoring for Climate Change (GMCC, Bodhaine, 1983) and Global Atmosphere Watch (GAW, Rose et al., 2021). The particle number concentrations (PNCs) and size distributions (PNSDs), considered to be primary indicators of human impacts on atmospheric composition, were the main aerosol properties measured at the networks. Based on long-term in situ measurements at the network sites, many studies on particle number and size distributions have been conducted since the 1990s in Europe and North America (Asmi et al., 2011; Birmili et al., 2016; Dal Maso et al., 2008; Heintzenberg et al., 2011; Krecl et al., 2017; Kulmala et al., 2004; Makela

et al., 1997; Sun et al., 2020; Wiedensohler et al., 2012). Their studies indicated that the annual, weekly and diurnal cycles largely depended on station type and geographic location. The more recent study of Schmale et al. (2018) also well illustrated the importance of measuring the PNSD over long-enough time periods in contrasting micro-environments for the understanding of aerosol–climate interactions and the improvement of their representation in numerical models. Sun et al. (2020) determined long-term trends of PNCs during 2009–2018 for 16 sites ranging from roadside to high-Alpine environments, and the annual relative slope varied from  $-17.2\%$  to  $-1.7\%$ ,  $-7.8\%$  to  $-1.1\%$  and  $-11.1\%$  to  $-1.2\%$  per year for 10–30, 30–200 and 200–800 nm size bins, respectively. The downward trends of PNCs were found to be dominated by the reductions in various anthropogenic emissions, while meteorology impacts were less important or negligible. However, a few long-term PNSD measurements in the developing countries mainly concentrated on urban Beijing since 2004 (Wang et al., 2013; Wehner et al., 2004), the North China Plain since 2008 (Shen et al., 2011) and Mount Waliguan since 2005 (Kivekas et al., 2009). Aitken mode particles (25–100 nm) were found to account for about half of total PNCs in urban areas in China (Wu et al., 2008), and the number of accumulation mode particles (100–1000 nm) was around 4 times higher than that in developed countries (Wehner et al., 2008; Wu et al., 2008), indicating largely different PNSD characteristics in China compared to Europe and North America.

PM<sub>2.5</sub> (particulate matter with aerodynamic diameter less than 2.5  $\mu\text{m}$ ) decreased by 30%–50% across China over the 2013–2018 period in response to the Air Pollution Prevention and Control Action Plan (APPCAP) in 2013 implemented by the Chinese central government (Zhai et al., 2019). Compared to PM<sub>2.5</sub> mass concentrations, the particle number concentrations were more directly affected by newly formed particles (Dal Maso et al., 2008; Dinoi et al., 2021), and new particle formation (NPF) events contributed about 54% of total PNCs in Leipzig, Germany (Ma and Birmili, 2015). Guo et al. (2014) tried to reveal the causal connection between NPF and haze pollution and reported that NPF trends precede winter haze episodes in Beijing. The more recent study by Kulmala et al. (2021) found that over 65% of the number concentrations of haze particles resulted from NPF events in Beijing, and their findings suggested that almost all present-day haze episodes originated from NPF, mainly since primary emission considerably decreased during recent year. PNSDs were considered to be better indicators of the strength of emission sources (Vu et al., 2015), but they were more easily modulated by aerosol dynamic processes, such as nucleation, coagulation, volatilization and condensation (Birmili et al., 2010; Kulmala, 2003). Nucleation and coagulation were largely affected by the coagulation sink (CoagS), and CoagS significantly decreased due to the large reduction of PM<sub>2.5</sub> mass concentrations in response to APPCAP. Therefore, the response of particle number concentration in differ-

ent size bins to emission mitigation policies may be different from PM<sub>2.5</sub> mass concentration.

The long-term PNSDs measurements were mainly conducted before APPCAP in China, and the response of particle number concentrations to the strictest ever air pollution control policies implemented by the Chinese central government has not been widely reported. Lanzhou, as one of the most polluted cities around the world with special basin terrain, won the Award for Today's Transformative Step 2015 awarded by the United Nations due to significant improvement in urban air quality (Zhao et al., 2018). The atmospheric horizontal and vertical dispersion conditions inside the basin are poor due to weak winds and strong multi-layer temperature inversion induced by basin terrain (Pandolfi et al., 2014). Therefore, the air pollutants were easily trapped inside the basin and hard to disperse to the upper air. Furthermore, basin aerosol pollution was more controlled by vertical than horizontal dispersion compared to the plain (Zhao et al., 2019). Based on a unique PNSD dataset for the period of 2012–2019 in urban Lanzhou in western China, this study investigates the long-term trends of PNCs in different modes to evaluate the role of emission reduction and meteorology in PNC variations. The results of this study may be important for the policymakers to cooperatively prevent and control heavy particle mass and number concentrations in Chinese megacities.

## 2 Data and methods

### 2.1 Measurement site descriptions

Lanzhou, located at the intersection of the Tibetan Plateau, the Loess Plateau and the Mongolian Plateau, is in a long valley running from the east to the west. The urban area is encircled by the hills rising from 200 to 600 m and thus forming saddle-shaped basin terrain (Fig. 1). The weak winds and multi-layer temperature inversion occurred frequently due to terrain impacts, and thus the air pollutants are trapped inside the basin (Chu et al., 2008). It was thought to be one of the most polluted cities around the world (WHO, 2018), and a photochemical smog episode (PSE) was observed in the 1980s at the Xigu District of urban Lanzhou, which was the first time a PSE was observed in China (Chen et al., 1986). The observation campaign was conducted from September 2012 to August 2019 on the rooftop of a 32 m high research building of the Northwest Institute of Eco-Environment and Resources (NIEER), Chinese Academy of Sciences. There are two major roads with a traffic volume of more than 2000 cars per hour near the observation site (Fig. 1). The NIEER is surrounded by residential and commercial buildings, with no local industrial sources around the site (Zhao et al., 2015a), and thus the measurement site can represent the urban background.

### 2.2 PNSD, criteria air pollutants and meteorology data

Five-minute particle number concentrations and size distributions (13–800 nm) were measured continuously using a scanning mobility particle sizer (Model 3936, TSI, USA) for about 7 years at the urban site from September 2012 to August 2019. The aerosol and sheath flow rates were set to 0.3 and 3 L min<sup>-1</sup>, respectively. The sampling inlet was mounted 1.5 m above the rooftop. The diffusional and gravitational losses for the inlet lines of the scanning mobility particle sizer (SMPS) were calibrated during the campaign. The SMPS's mobility was calibrated with monodisperse aerosols prior to their deployment in the field. The impactor was cleaned every day, and aerosol and sheath rates were examined with a bubble flow meter to ensure the good performance of the instrument. Each PNSD was parameterized with a least-squares log-normal fitting method providing parameters of two to three log-normal modes (Birmili et al., 2001). Three modes ( $i = 1, 2, 3$ ) were used: the nucleation mode (13–25 nm), the Aitken mode (25–100 nm) and the accumulation mode (100–800 nm). The log-normal distribution is expressed as (Seinfeld and Pandis, 2006)

$$\frac{dN}{d \log D_p} = \sum_{i=1}^n \frac{N_i}{\sqrt{2\pi} \log \sigma_i} \exp\left(-\frac{(\log D_p - \log \bar{D}_{p,i})^2}{2(\log \sigma_i)^2}\right), \quad (1)$$

where  $N_i$  is the total number concentration of the mode  $i$ ,  $\bar{D}_{p,i}$  is the median diameter of mode  $i$ ,  $\sigma_i$  is the geometric mean standard deviation of the distribution and  $n$  is the number of the modes. In this study “log” means log 10.

The hourly averaged concentrations of the criteria air pollutants (PM<sub>2.5</sub>, PM<sub>10</sub>, SO<sub>2</sub>, NO<sub>2</sub>, O<sub>3</sub>, CO) were measured at the Lanzhou Biological Preparations Institute, which is around 2.8 km away from the observation site. SO<sub>2</sub>, NO<sub>2</sub>, CO and O<sub>3</sub> are measured by the ultraviolet fluorescence method, the chemiluminescence method, the non-dispersive infrared absorption method and the UV-spectrophotometry method, respectively. PM<sub>2.5</sub> and PM<sub>10</sub> are measured by the micro-oscillating balance method. The 10 min meteorological parameters including temperature, relative humidity, wind speed and direction, precipitation and raindrop size distribution, and solar radiation were monitored by an automatic meteorological station co-located with the observation site. All the online data were hourly averaged and are presented in local time (China standard time = UTC + 8) throughout this paper.

### 2.3 Identification of NPF events and calculation of the relevant parameters

Referring to the methods presented in Dal Maso et al. (2005), NPF events were identified for a day. Number concentration sharply increased in the nucleation mode size range (13–25 nm) and prevailed for at least 1 h. Additionally, the particle size was required to increase during the next few hours. The parameters describing NPF events such as formation and

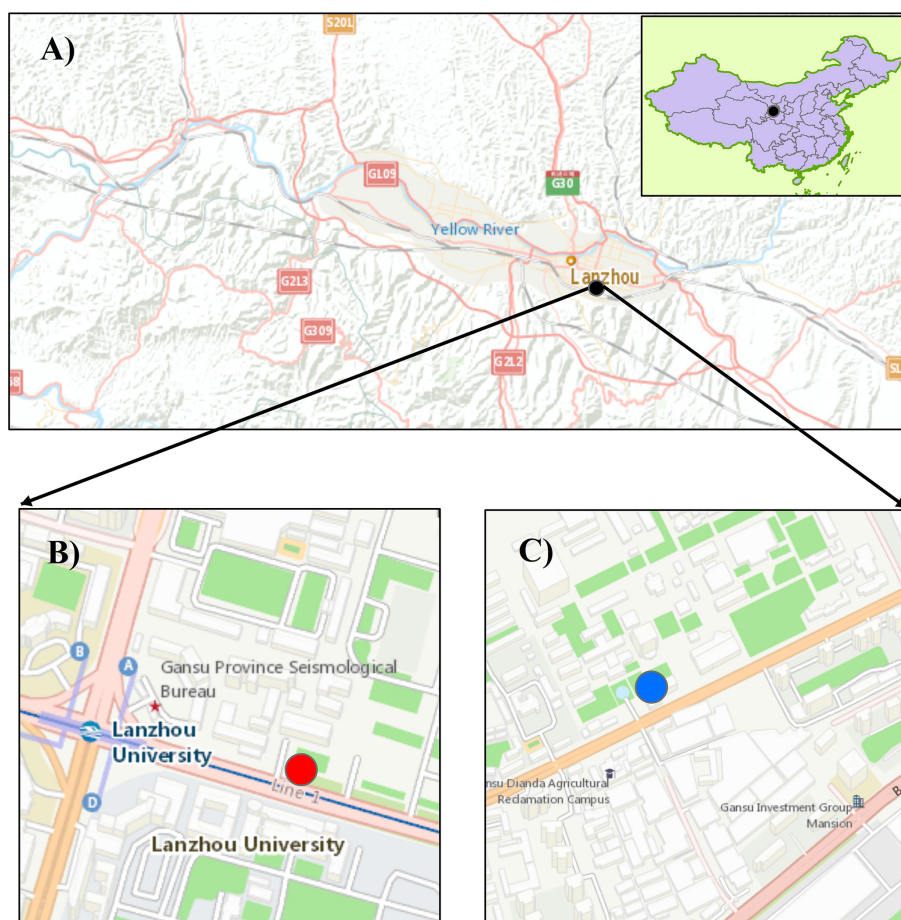


**Figure 1.** Map of (a) Lanzhou city, (b) the sampling site (red dot), and (c) the reference station that measured  $\text{PM}_{2.5}$  and  $\text{O}_3$  (blue dot). The map is a pure reproduction of Google Maps with added marks for our study locations. Copyright © Google Maps.

growth rates ( $J_D$  and GR hereafter) and condensation and coagulation sinks (CS and CoagS hereafter) were calculated in this study. GR can be calculated with the time evolution of the geometric mean diameter (GMD) of the nucleation mode obtained by parameterizing PNSD, and it can be expressed as

$$\text{GR} = \frac{d\text{GMD}}{dt}. \quad (2)$$

The formation rates ( $J_D$ ) can be calculated by

$$J_D = \frac{dN_{\text{nuc}}}{dt} + F_{\text{coag}}, \quad (3)$$

where the first term in the right-hand side ( $dN_{\text{nuc}}/dt$ ) represents the observed change in the number concentration of newly formed particles (Zhao et al., 2021). The second term is the loss of newly formed particles induced by coagulation scavenging and can be obtained with

$$F_{\text{coag}} = \text{CoagS}_{\text{nuc}} N_{\text{nuc}}. \quad (4)$$

The coagulation sink of nucleation mode particles ( $\text{CoagS}_{\text{nuc}}$ ) is defined as

$$\text{CoagS}(D_p) = \int K(D'_p, D_p) n(D'_p) dD'_p, \quad (5)$$

where  $K(D'_p, D_p)$  is the coagulation coefficient of particles with sizes of  $D_p$  and  $D'_p$ , calculated by the method of Fuchs (1964). The reference size ( $D_p$ ) is assumed to be the GMD of the nucleation mode. An average  $\text{CoagS}_{\text{nuc}} N_{\text{nuc}}$  over each formation period was taken during the campaign.

The condensation sink (CS) can be expressed as

$$\text{CS} = 2\pi D \sum \beta_m(D_{p,i}) D_{p,i} N_i, \quad (6)$$

where  $D_{p,i}$  and  $N_i$  are the particle diameter and the corresponding number concentration in size class  $i$ .  $D$  is the diffusion coefficient of the condensing vapor, usually assumed to be sulfuric acid.  $\beta_m$  represents a transition-regime correction (Kulmala et al., 2012),

$$\beta_m = \frac{1 + Kn}{1 + 1.677Kn + 1.333Kn^2}, \quad (7)$$

defined as a function of the Knudsen number,  $Kn = 2\lambda/D_{p,i}$ . Furthermore, based on the method presented in Dada et al. (2020), the  $\text{H}_2\text{SO}_4$  proxy was calculated to estimate the changes in the NPF precursors over the study period, and the equation is given as follows:

$$[\text{H}_2\text{SO}_4] = -\frac{\text{CS}}{2 \cdot (9.9 \times 10^{-9})} + \left[ \left( \frac{\text{CS}}{2 \cdot (9.9 \times 10^{-9})} \right)^2 + \frac{[\text{SO}_2]}{(9.9 \times 10^{-9})} \left( 1.6 \times 10^{-9} \cdot \text{GlobRad} \right) \right]^{1/2}, \quad (8)$$

where CS is calculated by Eq. (6).  $\text{SO}_2$  concentrations are measured using the ultraviolet fluorescence method, and global radiation (GlobRad) was measured by an SMP3 pyranometer (Kipp and Zonen, the Netherlands) during the campaign. In addition, the peak sizes of PNSDs are determined as mode diameters.

## 2.4 Trend analysis methods

Referring to the method used in the study of Sun et al. (2020), a customized Sen–Theil trend estimator was used to analyze the long-term trends of PNCs in nucleation, Aitken, and accumulation modes; the concentrations of the criteria air pollutants; and meteorological parameters in this study. The technique can calculate the true slope of the parameters by considering the impact of their seasonal, weekly, and diurnal cycles and avoid the effect of outliers and missing values. The change rates for the hourly or daily time series can be calculated with

$$m_{i,k} = \frac{(x(i + \Delta t) - x(i))}{\Delta t}, \quad (9)$$

where  $k$  is the integer.  $\Delta t$  is equal to the product of  $k$  and 364 d (52 weeks), indicating that data points from two different years are compared only if they were measured in the same hour of the day, day of the week and season the year.

## 2.5 Cluster analysis methods

To extract some more valuable information, the  $k$ -means clustering method used in various studies has been considered to be a preferred technique for data analysis in environmental fields (Sabaliauskas et al., 2013; Tunved et al., 2004). The  $k$ -means clustering routine split the multi-dimensional data into predefined number of subgroups, with clusters as different as possible from each other but as homogeneous as possible within themselves, by iteratively minimizing the sum of squared Euclidean distances from each member to its cluster centroid. Cluster analysis was used to divide hourly mean PNSDs during the campaign into several groups with comparable particle numbers in different size bins within

groups. The  $k$ -means clustering algorithm available in MATLAB® was used in this study. Based on the rule with maximum inter-cluster and minimum intra-cluster variances, the determination of the number of clusters, a very complicated problem, was conducted using the statistical software SAS® in this study, which is detailed in the study of Zhao et al. (2016).

## 3 Results and discussion

A continuous 7.5-year dataset was evaluated in this investigation. Except for the instrument maintenance and relocation, 80 % of the data were effective. The continuous PNSD dataset was integrated to calculate PNCs in different size bins. In this study, diameter ranges for the nucleation mode, Aitken mode and accumulation mode were determined as 13–25, 25–100 and 100–800 nm, respectively (Dal Maso et al., 2005). The total PNCs covered from 13 to 800 nm in mobility diameter.

### 3.1 Overview of the particle number concentration

Sources and origins of particles in the three modes may largely vary in specific micro-environments. Nucleation mode particles are from atmospheric nucleation events which are closely related to the low-volatility condensable gases such as water and sulfuric acid and growth of the smaller aerosol particles (Kulmala, 2003). Aitken mode particles are primarily emitted from combustion processes, such as coal combustion for domestic heating in wintertime and also from hygroscopic growth and coagulation of nucleation mode particles. For a relatively clean environment, the growth of nucleation mode particles is predominant due to a smaller coagulation sink (Rose et al., 2021), while the primary emissions are more important at the highly polluted urban areas (Hussein et al., 2004). Accumulation mode particles originate from the coagulation and hygroscopic growth of Aitken mode particles and long-range transport from the highly polluted areas.

Figure 2 shows variation of particle number in nucleation mode ( $N_{13-25}$ ), Aitken mode ( $N_{25-100}$ ), and accumulation mode ( $N_{100-800}$ ); aerosol optical properties (AOD, Alpha); criteria air pollutants ( $\text{PM}_{2.5}$ ,  $\text{O}_3$ ,  $\text{SO}_2$ , and  $\text{NO}_2$ ); and basic meteorological parameters (wind speed, relative humidity, temperature, net radiation) during the entire measurement campaign. The probability density functions and the corresponding statistical parameters are also given in Fig. 2. The mean  $\text{PM}_{2.5}$  and  $\text{O}_3$ ,  $\text{SO}_2$ , and  $\text{NO}_2$  concentrations were 49.9, 44.8, 22.7 and 57.5  $\mu\text{g m}^{-3}$  during 2014–2019, and mean values of wind speed, temperature, relative humidity and net radiation were 1.6  $\text{m s}^{-1}$ , 10.9 °C, 44.6 % and 44.4  $\text{W m}^{-2}$ , respectively. The mean values for  $N_{13-25}$ ,  $N_{25-100}$  and  $N_{100-800}$  were 2514.0, 10 768.7 and 3258.4  $\text{cm}^{-3}$ , respectively. Aitken mode particles, account-

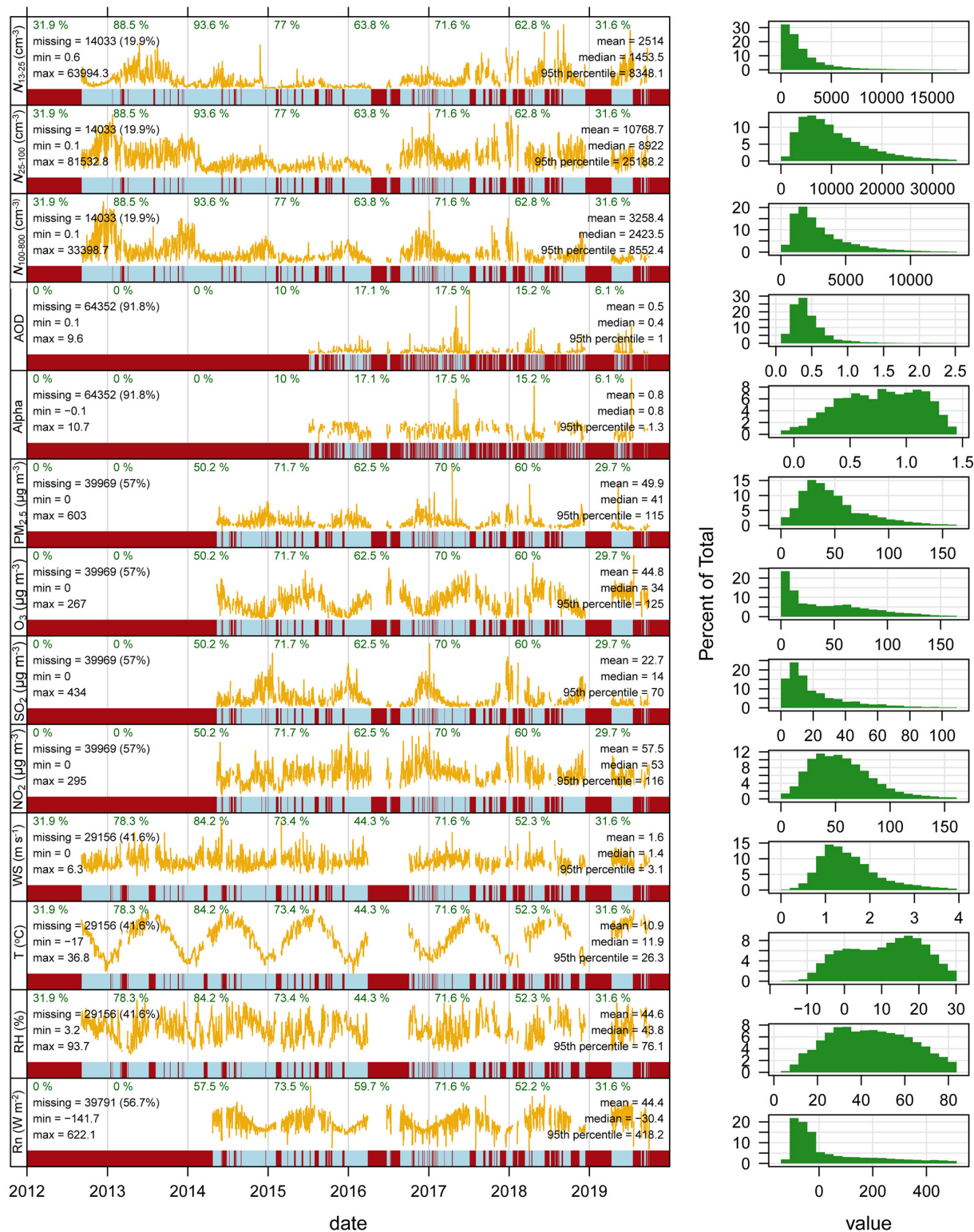


**Figure 2.** Time series of daily average particle number in the three modes ( $N_{13-25}$ ,  $N_{25-100}$  and  $N_{100-800}$ ), aerosol optical properties (AOD, Alpha), the criteria air pollutants ( $PM_{2.5}$ ,  $O_3$ ,  $SO_2$ ,  $NO_2$ ), and basic meteorological parameters and the corresponding probability density functions in urban Lanzhou during the campaign. The frequencies of missing values and the statistics are shown in each subplot.  $T$ , RH and  $R_n$  represent temperature, relative humidity and net radiation, respectively.

ing for 65.1 % of total PNCs, were significantly higher than the other modes, and the differences were much larger than the results in European cities (Cusack et al., 2013; Leoni et al., 2018), urban Beijing (Wu et al., 2008) and the North China Plain (Shen et al., 2011), which may be related to the fact that the particles at 3–12 and 800–1000 nm were not covered in nucleation and accumulation modes for our measurement campaign. The average particle number size distribution (PNSD) surface plots in four seasons for each year during the campaign are presented in Figs. S1–S4 to highlight the overall similarities and differences of each year during the study period. The mode diameter of PNSD shifted to smaller particle size in four seasons from 2012 to 2019. The particle number in Aitken and accumulation modes declined significantly in autumn and winter during the study periods, which could be due to the strictest emission control policies in recent years. However, in spring and summer, the nucleation mode particle number increased significantly after 2016, which can be partly modulated by NPF events. The impacts of emission control and NPF events are discussed in the following sections in more detail.

Until now, numerous measurements of sub-micron PNSDs have been carried out at a variety of locations to examine their variations and key influencing factors. Table 1 summarizes experimentally determined particle number concentrations in the troposphere for the measurement campaigns conducted over time periods longer than 1 year across the globe. The mean number concentrations in the three modes were much lower than those in urban Beijing (Wang et al., 2013) and significantly higher than those at a remote background station, Mt. Waliguan, one of the global GAW sites in China (Kivekas et al., 2009). The sub-micron particle number concentration was much lower compared to the most polluted cities in India, such as Delhi (Gani et al., 2020) and Kanpur (Kanawade et al., 2014), especially for Aitken and accumulation modes. The number of particles in Aitken and accumulation modes at Asian cities were even higher than those at the urban sites in Europe and North America, which may largely be related to poor visibility in Asian cities according to Mie scattering theory. For nucleation mode, the situation is the opposite, which may be because newly formed particles were rapidly scavenged by coagulation with larger particles in highly polluted cities (von Bismarck-Osten et al., 2013; Wang et al., 2011).

### 3.2 Trends of PNCs, criteria air pollutants and meteorological parameters

Besides primary emissions from human activities in urban areas, particle number concentration was easily affected by secondary newly formed particles, which were closely related to meteorological conditions such as temperature, relative humidity and new radiation (Zhao et al., 2015a). Figure S5 shows inter-annual variations of monthly averaged particle numbers, criteria air pollutants, and wind speed during

2012–2019, and it normalizes the time series data ( $N_{13-25}$ ,  $N_{25-100}$ ,  $N_{100-800}$ ,  $PM_{2.5}$ ,  $O_3$ ,  $SO_2$ ,  $NO_2$  and wind speed) to fix values to equal 100 at the beginning of September 2012. The particle number in the three size ranges declined largely during 2012–2015 (Period I), and summer  $N_{13-25}$  decreased by around 75 % in 2015 compared to that in 2013, while that in winter varied less during Period I. The  $N_{25-100}$  and  $N_{100-800}$  reduced more in winter than in summer due to emission control impacts. The number of nucleation mode particles ( $N_{13-25}$ ) increased significantly during 2016–2019 (Period II), which was consistent with  $O_3$  while showing the opposite trend with declining  $PM_{2.5}$  during Period II. The strongly declining aerosol radiative effect due to the strict air pollution controls resulted in an unprecedented rapid increasing trend in surface solar radiation over China during 2014–2019 (Shi et al., 2021), which may promote the formation of secondary air pollutants.

The particle number in the Aitken and accumulation modes ( $N_{25-100}$ ,  $N_{100-800}$ ) firstly increased during 2016–2017 and then decreased from 2018 to 2019, and their variations were consistent with the primary emitted pollutants ( $SO_2$ ,  $NO_2$ ), indicating that  $N_{25-100}$  and  $N_{100-800}$  variations during 2016–2018 were mainly modulated by primary emissions. Sun et al. (2020) analyzed the long-term trends of particle number concentrations at 16 observational sites in Germany from 2009 to 2018, and number concentrations of particles in the three modes were found to have significant decreasing trends in response to emission mitigation policies. The contrasting response of nucleation mode particles to mitigation policies between China and Germany may be related to the fact of the increased reduction of the coagulation sink due to the strictest ever clean air action plan in China, and thus NPF event occurred easily due to the lower coagulation scavenging effects (Gani et al., 2020). The variation in wind speed was not significant during the entire measurement campaign.

In view of the contrasting PNC trends between periods I and II, the following analyses compared mean diurnal and annual variations of particle number in the three size bins ( $N_{13-25}$ ,  $N_{25-100}$  and  $N_{100-800}$ ),  $PM_{2.5}$  and  $O_3$  as wind directions before and after January 2016 (Figs. 3, S6–S9). The most obvious increase in  $N_{13-25}$  was during 12:00–16:00 in the summer months after January 2016 compared to before January 2016, and the largest increase corresponded to easterly, southerly and southwesterly winds, especially for the annual cycles with the more significantly increased  $N_{13-25}$  for southeasterly winds. The large conditional probability function (CPF) values of  $N_{13-25}$  mainly corresponded to southerly winds (Fig. S10), which can support the above results. The  $N_{25-100}$  difference between the two periods (2012–2015 vs. 2016–2019) was much less significant than  $N_{13-25}$ , and the most obvious  $N_{25-100}$  increase occurred in morning and evening rush hours for northeasterly winds (Fig. S6), which could be supported by the results of polar plots (Fig. S10). Figure 4 illustrates mean particle number

**Table 1.** Overview of experimentally determined particle number concentrations in the troposphere around the world. The duration of the measurement campaign was at least longer than 1 year (12 months).

Continent	Diameter, city, site and period	Number concentrations			Reference
Asia	Diameter range (nm)	13–25	25–100	100–800	This work
	Lanzhou, urban, 7.5 years	2514	10 769	3258	
	Diameter range (nm)	3–20	20–100	100–800	Wang et al. (2013)
	Beijing, urban, 3 years	5000	12300	6400	
	Diameter range (nm)	12–21	21–95	95–570	Kivekas et al. (2009)
	Waliguan, remote rural, 22 months	570	1060	430	
	Diameter range (nm)	3–25	25–100	100–1000	Shen et al. (2011)
Shangdianzi, rural, 1.5 years	3610	4430	3470		
Europe	Diameter range (nm)		20–100	100–685	Kanawade et al. (2014)
	Kanpur, urban, 4 years		12400	18 900	
	Diameter range (nm)	12–25	25–100	100–560	Gani et al. (2020)
	Delhi, urban, 1.25 years	8940	21 690	11 690	
	Diameter range (nm)	8–25	25–90	90–460	Dal Maso et al. (2008)
	Värriö, rural, 3 years	143	429	304	
	Diameter range (nm)	8–30	30–100	100–700	von Bismarck-Osten et al. (2013)
Copenhagen, rural, 3 years	770	1813	751		
Diameter range (nm)	8–30	30–100	100–700	von Bismarck-Osten et al. (2013)	
Leipzig, roadside, 3 years	5692	4962	2242		
Diameter range (nm)	8–30	30–100	100–700	von Bismarck-Osten et al. (2013)	
Helsinki, urban background, 3 years	3080	3099	1053		
Diameter range (nm)	8–30	30–100	100–700	von Bismarck-Osten et al. (2013)	
London, urban background, 3 years	1632	3825	1437		
North America	Diameter range (nm)	10–50	50–100	100–500	Wang et al. (2011)
	Rochester, urban, 8 years	4730	1838	1073	
	Diameter range (nm)	3–20	20–100	100–1000	Stanier et al. (2004)
Pittsburgh, urban, 1 year	9700	10 100	2188		

size distributions by varying wind directions, and the number of Aitken mode particles for north northeasterly winds (0–45 °C) was higher than that for the other wind directions. The emissions from jammed traffic and winter domestic heating with traditional stoves at Keji Street, about 500 m away from the sampling site, could be transported to the station as northeasterly winds. In addition, the larger increase in  $N_{25-100}$  at 13:00 for easterly, southerly and southwesterly winds was consistent with  $N_{13-25}$  possibly due to newly formed particle growth impacts.

The  $N_{100-800}$  and  $PM_{2.5}$  trends from Period I to II in diurnal and annual cycles were opposite to those in  $N_{13-25}$  with a significant reduction at noon in the summer months for southerly winds (Figs. S7, S8 and S10), which were mainly affected by the clean air action plan (Li et al., 2021). Gani et al. (2020) studied particle number concentrations and size distributions in the polluted megacity of Delhi in In-

dia and pointed out that strategies that only target accumulation mode particles (which constitute much of the fine  $PM_{2.5}$  mass) may even lead to an increase in the UFP concentrations as the coagulation sink decreases. Furthermore,  $O_3$  increased more significantly in the afternoon in summer months after January than before January 2016, and wind directions for the largest increased  $O_3$  concentrations were consistent with nucleation mode particles (Fig. S9), which further confirmed that the increased  $N_{13-25}$  from Period I to II was induced by more frequent nucleation events. Compared to before January 2016, the more favorable meteorological conditions after January 2016 such as the much drier air (Fig. S5), higher ambient temperature (Fig. S5) and stronger solar radiation (Fig. S12) for southerly winds also helped to form new particles, which could be supported by our previous work in the same site (Zhao et al., 2015a).

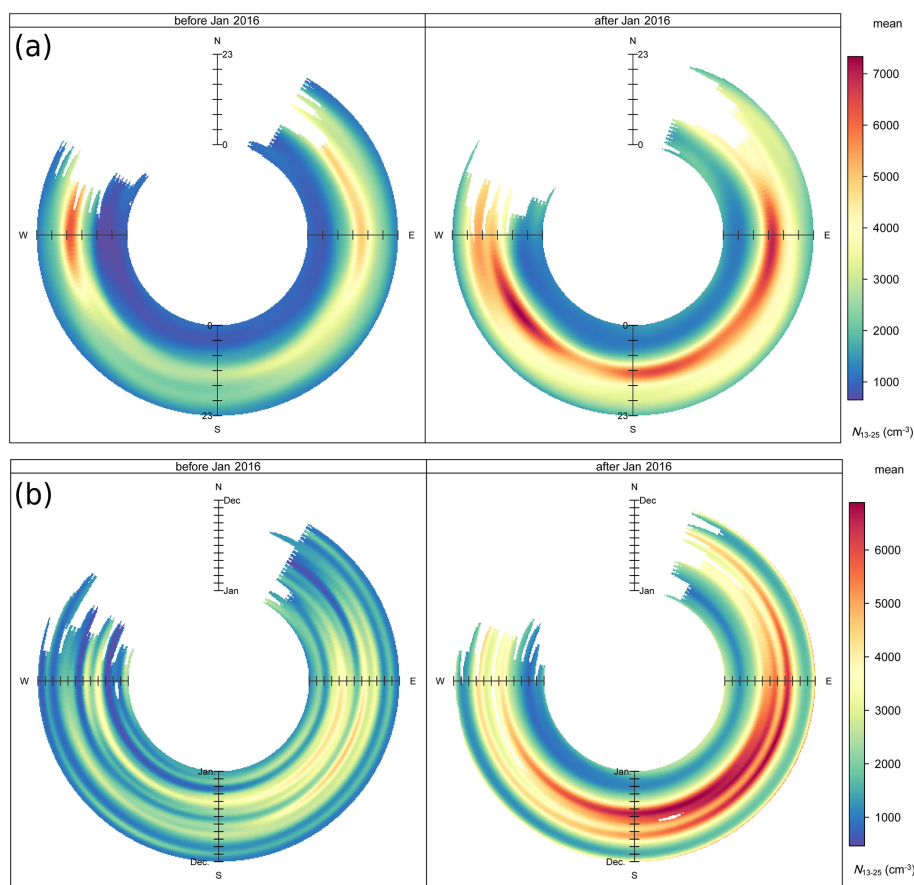


**Figure 3.** Mean diurnal (a) and annual (b) variations of particle number in 13–25 size bins ( $N_{13-25}$ ) as wind directions in the two contrasting periods (before vs. after January 2016).

### 3.3 Typical particle number size distributions influenced by varying factors

Besides the chemical composition of airborne particles, the information derived from particle number size distributions (PNSDs) is beginning to play an important role in source apportionment studies (Vu et al., 2015) due to the obvious difference in diameters for the particles from varying sources. The hourly average PNSDs during the entire measurement campaign were classified into six clusters by the  $k$ -means clustering technique, and the mean PNSD for each typical type was shown in Fig. 5. As shown in Fig. 5, the shape and mode diameter of PNSDs were largely different among the clusters. Mode diameters varied from  $\sim 20$  nm for Cluster B to 70 nm for Cluster F, and more than a quarter of PNSDs were sorted into Cluster A with a mode diameter of  $\sim 55$  nm, while Cluster B occurred less frequently with a mode diameter of  $\sim 20$  nm. The sources and key factors influencing each cluster of PNSD can be better determined by average annual and diurnal variations of occurrence frequencies, as well as the corresponding air pollutants and meteorological parameters for the clusters (Fig. 6, Tables 2 and 3).

About 70% of clusters A and F are in the cold seasons (October–December and January–March) with the almost opposite diurnal pattern between the two clusters (Fig. 6). Clusters A and F had the highest number concentrations of accumulation mode particles ( $N_{100-800}$ ) and mass concentrations of particulate matter ( $\text{PM}_{2.5}$ ,  $\text{PM}_{10}$ ) and gaseous pollutants ( $\text{SO}_2$ ,  $\text{NO}_2$ , CO), while they had the lowest particle number concentrations in nucleation mode ( $N_{13-25}$ ) and  $\text{O}_3$  mass concentrations among the clusters (Table 2), suggesting that the two polluted clusters may be mainly impacted by primary emissions from human activities, which is defined and abbreviated as Pollut\_C in the following analyses. This can also be confirmed by the larger geometric median diameters for the three modes ( $\text{GMD}_{\text{nuc}}$ ,  $\text{GMD}_{\text{Ait}}$  and  $\text{GMD}_{\text{acc}}$ ) compared to the other clusters, as well as the high particle number concentrations in the morning and evening rush hours (Fig. S13). Compared to other clusters, the weaker winds and net radiation, lower ambient temperature, and higher relative humidity indicated that the severe air pollution for clusters A and F was significantly affected by stable air and poor diffusion conditions. Furthermore, as illustrated in Fig. 7, Cluster F (A) accounted for more than 40% (60%) of all clusters.

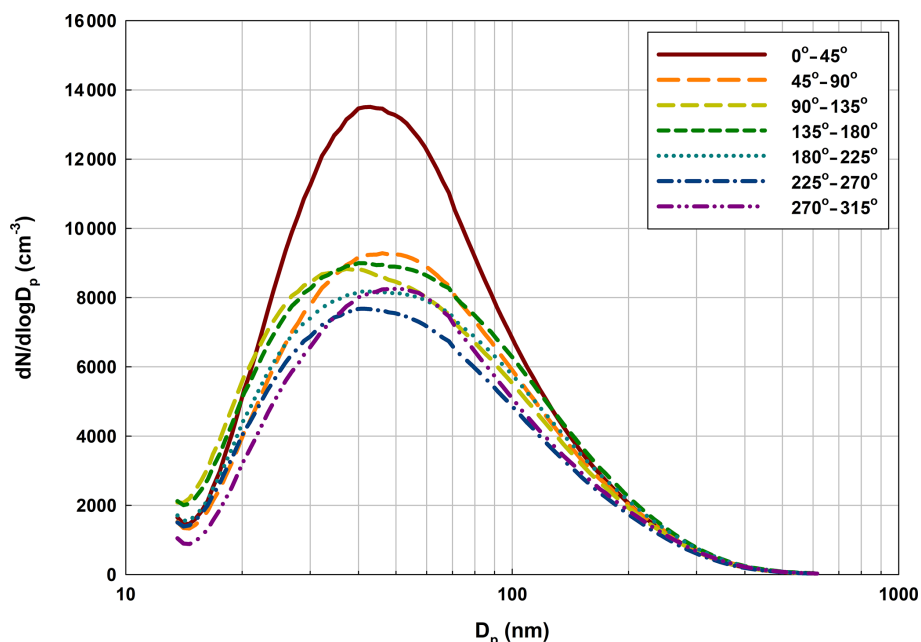


**Figure 4.** Mean particle number size distributions by each sector of wind directions with an interval of 45° during 2012–2019.

**Table 2.** Mean values of particle number in the three modes ( $N_{13-25}$ ,  $N_{25-100}$  and  $N_{100-800}$ ), AOD, the concentrations of six criteria air pollutants ( $PM_{2.5}$ ,  $PM_{10}$ ,  $O_3$ ,  $SO_2$ ,  $NO_2$  and  $CO$ ) and the condensation sink (CS) for each cluster.

Cluster units	$N_{13-25}$ $cm^{-3}$	$N_{25-100}$ $cm^{-3}$	$N_{100-800}$ $cm^{-3}$	AOD –	$PM_{2.5}$ $\mu g m^{-3}$	$PM_{10}$ $\mu g m^{-3}$	$O_3$ $\mu g m^{-3}$	$SO_2$ $\mu g m^{-3}$	$NO_2$ $\mu g m^{-3}$	$CO$ $mg m^{-3}$	CS $10^{-3} s^{-1}$
A	1263.2	12 156.5	3973.9	0.54	54.85	135.73	25.98	26.91	64.57	2.91	3.64
B	10 370.4	9969.8	1504.7	0.39	31.42	86.53	92.77	13.56	40.67	2.73	13.8
C	2616.7	9071.8	2890.5	0.49	48.89	116.10	41.37	21.42	55.12	2.65	4.42
D	2010.0	11 931.4	2301.6	0.55	43.92	124.13	46.28	16.85	57.68	2.33	5.33
E	4245.2	10 806.9	1592.6	0.45	35.26	106.31	82.86	12.60	44.44	1.71	7.88
F	757.2	9492.2	5139.3	0.60	71.24	130.98	24.14	35.95	66.07	2.98	2.12

ters during 5 h after the occurrence of Cluster A (F), and the more frequently synchronous occurrence between clusters A and F may be related to the pollution process from light–severe–light episodes. From the perspective of inter-annual variations in occurrence frequency, Pollut\_C occurred increasingly less frequently from 2014 to 2019, possibly due to implementation of the clean air action plan (Fig. 6a), which is analyzed in detail in the following section.

The clusters B and E mainly appeared in the daytime in the warmer months, and the occurrence frequency had a sharp peak in the afternoon (Fig. 6b, c), but the peak for Cluster E lagged by around 2 h compared to that for Cluster B. The frequency of Cluster E during 2 h after the occurrence of Cluster B was larger than 80 %, and the mode diameter of Cluster E ( $\sim 30$  nm) was only larger than that of Cluster B ( $\sim 20$  nm); thus, it was inferred that Cluster B represented secondary new particle formation (NPF) event impacts, while Cluster E was influenced by subsequent new

particle growth events. The inference could be confirmed by the highest particle number in nucleation mode and  $O_3$  mass concentration among the clusters (Table 2). The sharply increased nucleation mode particles at 09:00 were followed by a subsequent growth to accumulation mode indicated by the typical banana-shaped temporal development of the number size distribution (Fig. S13, Boy and Kulmala, 2002), which also supported the above inference. In addition, the reduced coagulation sink and low number concentrations of particles in accumulation mode as well as low  $PM_{2.5}$  and  $PM_{10}$  mass induced by higher wind speed helped to form secondary new particles (Tables 2 and 3). The more recent study of Gani et al. (2020) investigated particle number concentrations and size distribution in a polluted megacity, Delhi, and found that reduction in mass concentration in the highly polluted megacity may not produce a proportional reduction in PNCs and may even lead to an increase in the UFP concentrations as the coagulation sink decreases. The mean AOD of 0.39

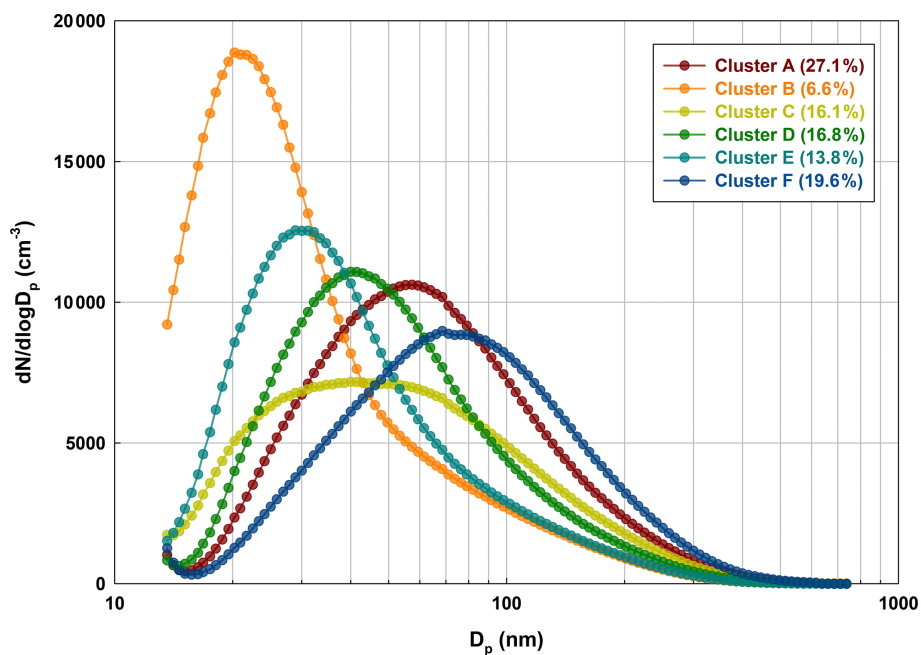


**Figure 5.** Mean particle number size distribution for each typical cluster obtained by the *k*-means clustering method. The occurrence frequencies of clusters A–F were calculated during 2012–2019.

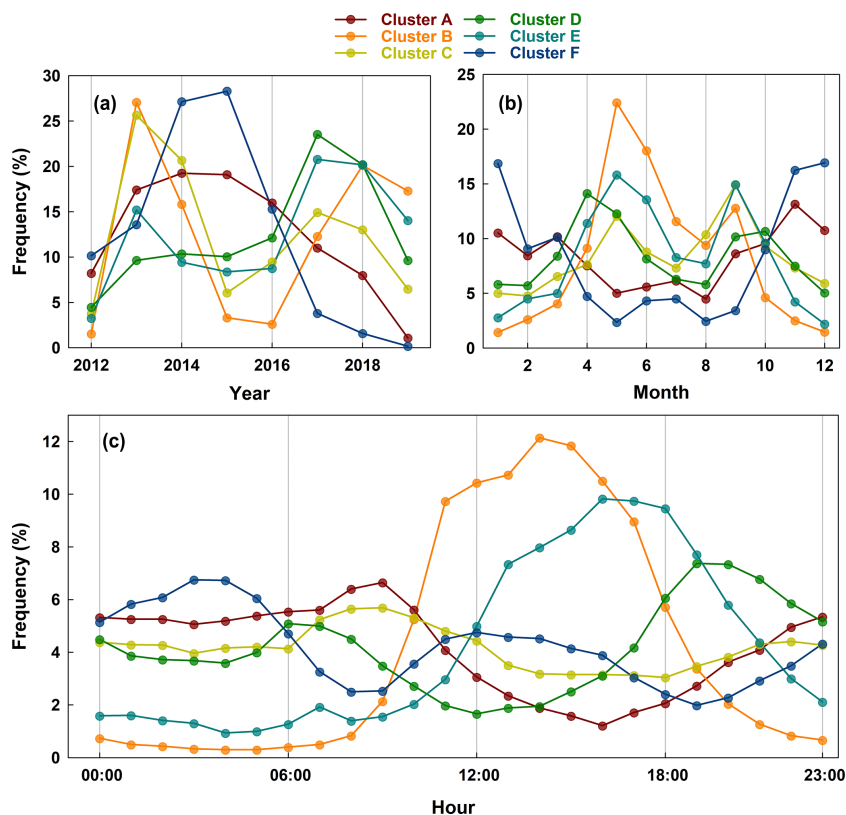


**Figure 6.** (a) Inter-annual, (b) average annual and (c) diurnal variations of occurrence frequencies for clusters A–F during the measurement campaign.

**Table 3.** Mean values of meteorological parameters (wind speed, temperature, relative humidity and net radiation) and geometric median diameters ( $GMD_{nuc}$ ,  $GMD_{Ait}$  and  $GMD_{acc}$  are for nucleation, Aitken and accumulation modes) fitted by Eq. (1) for each cluster. WS,  $T$ , RH and  $R_n$  are the abbreviations of wind speed, temperature, relative humidity and net radiation, respectively.

Cluster units	WS $m s^{-1}$	$T$ $^{\circ}C$	RH %	$R_n$ $W m^{-2}$	$GMD_{nuc}$ nm	$GMD_{Ait}$ nm	$GMD_{acc}$ nm
A	1.38	7.35	48.39	21.56	26.37	54.91	133.08
B	2.18	20.77	31.59	223.55	19.72	38.06	131.70
C	1.64	13.18	48.20	48.25	22.56	49.91	137.21
D	1.57	11.73	44.31	-3.03	25.73	44.33	128.89
E	1.94	17.47	36.19	100.16	23.18	38.74	122.96
F	1.34	5.34	47.03	12.82	25.69	62.35	136.55

for Cluster B was significantly lower than that for the other clusters (Table 2), which resulted in the higher atmospheric transparency and thus stronger net radiation ( $223.55 W m^{-2}$ ) and higher ambient temperature ( $20.77^{\circ}C$ ). The drier air was conducive to detecting NPF events, and newly formed particle growth was limited by hygroscopicity under low-RH environments. The occurrence frequency for the two clusters first decreased from 2013 to 2015 and then increased until 2019, which contrasted with Pollut\_C during the campaign. Clusters B and E were abbreviated as NPF\_C for the following analyses. The condensation sink (CS) ranged from  $2.12 \times 10^{-3} s^{-1}$  for Cluster F to  $1.38 \times 10^{-2} s^{-1}$  for Cluster B during the campaign (Table 2). The CS values for clusters B and F, representing new particle formation and growth events, were much higher than those for the other clusters, but they were even lower than CS during NPF events in the North China Plain ( $0.02 s^{-1}$ , Shen et al., 2011). Therefore, the large PNSD discrepancy among the clusters may be less influenced by the condensation sink during the measurement campaign. It is possible that CS was not a key factor in modulating the occurrence of NPF events in urban Lanzhou in western China and that NPF was mainly affected by meteorological variables and coagulation effects (Table 3).

The mean PNSD for Cluster C was much wider and more flat than that for the other clusters, and thus it was hard to determine the mode diameter, especially for the PNSDs from dawn to noon (Figs. 5 and S13). The number of particles in nucleation mode ( $N_{13-25}$ ) was only lower than NPF\_C, while that in accumulation mode ( $N_{100-800}$ ) was only lower than Pollut\_C. The cluster occurred more easily in the morning in the warm months, which was consistent with most of the clusters except the polluted clusters A and F. Additionally, except for Cluster F, the occurrence frequency of the other clusters was comparable and ranged from about 15 % to 28 % during 1–12 h after Cluster C. The frequency of Cluster C also varied less during 1–12 h after clusters A, D, E and F (Fig. 7). Combining this with the modest particle number concentrations in the three modes, criteria air pollutants and meteorological parameters, it was inferred that Cluster C represents the urban background PNSD, and thus it is de-

finied as UB\_C in the following analyses. Cluster D occurred more frequently in the morning and evening rush hours in the warm seasons (Fig. 6), and the corresponding mean particle number in Aitken mode ( $N_{25-100}$ ) was the second highest ever – just behind Cluster A, which may be impacted by motor vehicle emissions from the nearby roads. The mode diameter of  $\sim 40$  nm was only larger than NPF\_C (clusters A and E), and it appeared frequently after Cluster E with the high concentration of particles in Aitken mode in the afternoon (Fig. S13) possibly due to new particle growth impacts. Therefore, Cluster D was jointly influenced by motor vehicle emissions and NPF events and is defined as VE\_NPF\_C in the following section.

From the perspectives of the variation in mode diameter among the clusters (Fig. 5) and the variation in frequency during 1–12 h after each cluster (Fig. 7), the NPF\_C was closely followed by Pollut\_C during the measurement campaign, and the clusters can be ranked by temporal order as  $B \rightarrow E \rightarrow D \rightarrow A \rightarrow F$ . Therefore, NPF events significantly contributed to haze episodes in the subsequent 1–2 d, which may be increasingly obvious mainly due to considerably decreased emissions of primary particles during recent years in response to the clean air action plan. Guo et al. (2014) first reported that atmospheric NPF tends to precede winter haze episodes in Beijing, and then the latest study of Kulmala et al. (2021) investigated how NPF and subsequent particle growth affect the initial steps of haze formation in Beijing. Their findings showed that reducing the subsequent growth rate of freshly formed particles by a factor of 3–5 would delay the buildup of haze episodes by 1–3 d.

### 3.4 Impact of the clean air action plan on PNC variations

The response of  $PM_{2.5}$  mass to the clean air action plan has been evaluated in many previous studies, and  $PM_{2.5}$  was found to decrease by 30 %–50 % across China during 2013–2018 due to the implementation of emission control policies (Zhai et al., 2019). The impact of the policies on particle number may be more complex compared to PM mass since more fine particles cannot rapidly grow by coagulation with

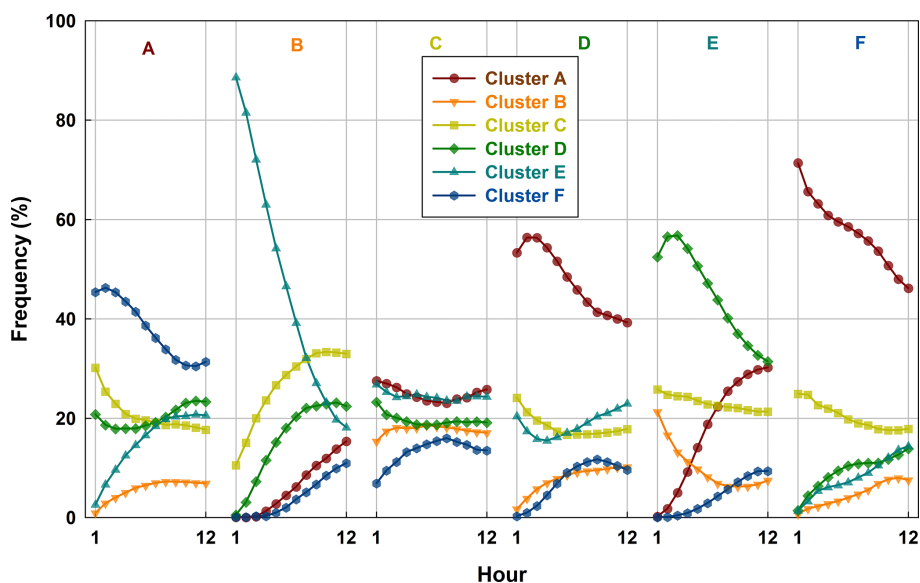


**Figure 7.** Occurrence frequency of the other clusters at the subsequent 1–12 h after each cluster appeared during the entire measurement campaign. For example, the frequencies of clusters B, C, D, E and F in the subsequent 1–12 h when Cluster A appeared (the first column of Fig. 7) can be calculated by the equation  $N_{A,i,j} = N_{i,j} / \sum N_i \times 100\%$  ( $i = 1, 2, \dots, 12$ ,  $j$  represents the other clusters except Cluster A, i.e., clusters B, C, D, E and F). The calculation is similar when the other clusters appeared during the campaign.

the reduced coarse particles (Gani et al., 2020). However, the response of PNCs to the restricted emissions was only analyzed by some short-term measurements during some important and international meetings and activities such as the Summer Olympic Games in 2008, the Asia-Pacific Economic Cooperation (APEC) in 2014 and China's Victory Day parade in 2015 (Chen et al., 2015; Shen et al., 2016; Wang et al., 2013). The long-term in situ measurements of PNSDs and mass concentrations of the criteria air pollutants were essential to understand the emission control impacts and to reveal the mechanism. Figures 8, S14 and S15 show the trends of daily mean particle number in the three modes as wind directions for each cluster based on 7.5 years of measurement. The number of particles in nucleation mode ( $N_{13-25}$ ) first decreased from 2012 to 2015 and then increased rapidly after 2016. The  $N_{13-25}$  changing trend for NPF\_C (clusters B and E) was more significant compared to that for the other clusters, especially for southeasterly winds. The specific winds corresponded to more  $\text{PM}_{2.5}$  reduction on summer afternoons after 2016 than before 2016 due to the impact of emission mitigation policies (Fig. S8), and thus NPF events, represented by NPF\_C, were easily detected by chemical reactions due to reduced coagulation sink. More solar radiation reached near-surface air as a result of reduced  $\text{PM}_{2.5}$  mass (Shi et al., 2021), and thus ambient temperature increased and relative humidity declined (Fig. S11), which also favored the occurrence of NPF events (Zhao et al., 2015a).

At our sampling site,  $N_{25-100}$  was easily influenced by growth of newly formed particles and primary emissions from human activities. The  $N_{25-100}$  trends were similar to

$N_{13-25}$  for clusters B, D and E, and the increasing trends were also more significant after 2016 for southwesterly winds (Fig. S14), which represented NPF impacts. Dependence of  $N_{25-100}$  on wind directions was not obvious for clusters A, C and F, and thus the trends may be related to variations in primary emissions. Unlike nucleation and Aitken modes, particle number in accumulation mode ( $N_{100-800}$ ) depended less on wind directions. Furthermore,  $N_{100-800}$  was the lowest and less varied for NPF\_C, while that for clusters A, C and D had a similar trend to  $N_{25-100}$ , and that for Cluster F, the most polluted cluster, had a downward trend during the campaign due to the implementation of the strictest ever the clean air action plan. Therefore, the response of particle number to air pollution control may be significantly different for each size fraction, which may be closely related to the variations in coagulation sink and meteorological conditions induced by reduced primary emissions. This is discussed in detail in the following section.

To better evaluate variations in particle number concentrations and emission control impacts, Figs. S16, S17 and S18 show variations of the contributions of each cluster to monthly averaged PNCs in 13–25, 25–100 and 100–800 nm during the campaign, respectively. Pollut\_C (clusters A and F) dominated the winter PNCs in different size bins before 2016, and their occurrence was less and less frequent after 2016, especially for the most polluted Cluster F, which was largely dominated by a reduction in primary emissions. In contrast to Pollut\_C, as a main cluster representing NPF events, the contribution of Cluster B to summer  $N_{13-25}$  decreased from 50 % to about 10 % during 2013 to 2015 and

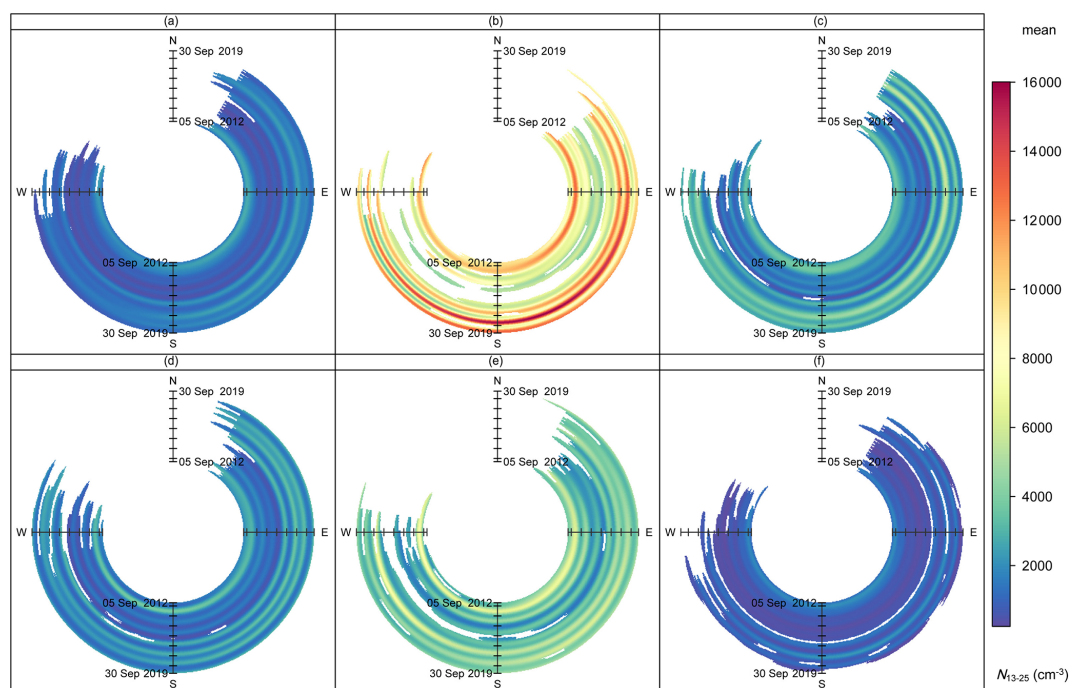


**Figure 8.** Trends of daily mean particle number in nucleation mode ( $N_{13-25}$ ) as wind directions for each cluster during the entire measurement campaign.

then increased to reach around 60% in 2019. For Cluster C representing urban background, its frequency varied less during the entire measurement campaign. The particle number was dominated by primary emissions before 2016, and thereafter that was controlled by NPF events, which was partly due to emission control. In response to air pollution control, the reduction in coarse particles could promote secondary new particle formation due to the reduced coagulation sink (Gani et al., 2020). NPF events were largely dependent on PM mass concentrations mainly contributed by coarse aerosol particles. Accumulation mode particle number concentrations in cities of developing countries are generally higher than those in many western cities (Gani et al., 2020; Wu et al., 2008), and thus the response of NPF events to emission control may be significantly different between the cities of developed and developing countries. For example, Sun et al. (2020) found coincidentally downward trends of particle number and black carbon mass concentrations at 16 observational sites in Germany from 2009 to 2018 due to reduced anthropogenic emissions. Gani et al. (2020) pointed out that strategies that only target accumulation mode particles in a polluted megacity in India may even lead to an increase in the UFP concentrations as the coagulation sink decreases. Shen et al. (2016) also found that  $PM_{10}$  mass concentration was significantly reduced while NPF event frequency was much higher during the short-term emission control period.

We also quantitatively evaluated the changing trends of particle number in the three modes by Theil–Sen regression. In view of the contrasting trends, the observation period was divided into two sub-periods, i.e., before and after January 2016. Figures 9 and 10 illustrate the seasonal and diurnal variations of the trends of PNCs for each cluster during each sub-period. For Period I (2012–2015), PNCs in the three size bins exhibited downward trends for all clusters, especially in spring. The annual relative slopes of spring PNCs varied from  $-54.7\%$  for Cluster F to  $-17.2\%$  for Cluster B, from  $-42.6\%$  for Cluster A to  $-14.1\%$  for Cluster B, and from  $-40.7\%$  for Cluster A to  $-17.5\%$  for Cluster B per year for 13–25, 25–100, and 100–800 nm size ranges (Fig. 9). The PNCs for Pollut\_C (clusters A and F) decreased by about 40% in the morning and evening rush hours, which was much higher than in the other hours of the day. Therefore, the increased reduction in PNCs for Pollut\_C may be closely related to emission control policies. The much larger PNC reduction in this study than in Germany may be due to the strictest emission mitigation policies ever implemented in Chinese cities (Sun et al., 2020). In contrast to Period I, the UFP number increased and the amplitude was greater during Period II (2016–2019). The annual relative slopes of  $N_{13-25}$  varied between 5.1% (fall) and 314.4% (winter), 8.0 (fall) and 135.5% (spring), 11.3% (fall) and 184.3% (winter),  $-4.5$  (fall) and 59.1% (summer), 6.3% (fall) and 30.3% (spring), and 3.6% (fall) and 15.7% (spring) for clusters A–F. The maximum increase of  $N_{13-25}$  was in the

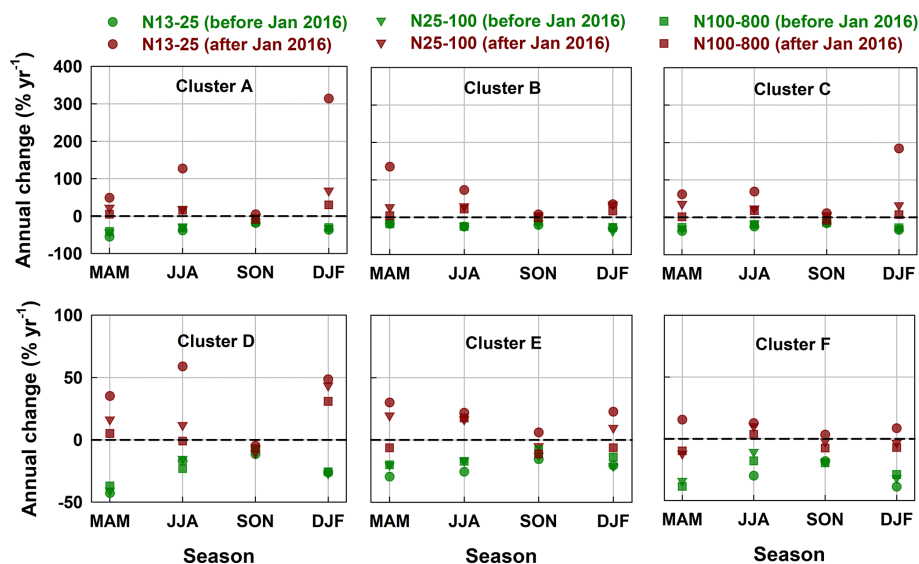


**Figure 9.** Seasonal variations in the trends of PNCs in three modes for the two contrasting periods (before vs. after January 2016) for each cluster. The annual change is calculated by Theil–Sen regression, and the calculation is shown in Sect. 2.4 (Trend analysis methods). MAM, JJA, SON and DJF refer to spring, summer, fall and winter, respectively.

spring afternoon for NPF\_C, which may be governed by NPF events due to the reduced coagulation sink corresponding to low  $N_{100-800}$ . The winter  $N_{13-25}$  increased significantly for Cluster A during Period II, especially in the morning and evening rush hours, suggesting the impact of primary emissions from motor vehicles. The annual slope of  $N_{100-800}$  varied less compared to that of ultrafine particles in seasonal and diurnal cycles.

To better analyze long-term trend of NPF events and the relevant parameters during 2012–2019, Fig. 11 illustrates the inter-annual statistics of the trends of NPF frequency, mode diameter, and formation and growth rates. Furthermore, condensation and coagulation sinks (CS, CoagS) and  $\text{H}_2\text{SO}_4$  proxy were also calculated over the study period. Similar to the opposite  $N_{13-25}$  trend between the two contrasting periods (Figs. 8–9), the occurrence frequency of NPF events decreased from  $\sim 30\%$  to less than  $5\%$  until 2016 and then increased to more than  $30\%$  in 2019. Particles have become much finer since 2015 due to more frequent NPF events (Fig. 11b). The temporal variations of PNCs in nucleation mode ( $dN_{\text{nuc}}/dt$ , Fig. 11c) and the coagulation scavenging effect ( $F_{\text{coag}}$ , Fig. 11d) followed similar inter-annual variations of NPF frequency. The contribution of coagulation loss flux  $F_{\text{coag}}$  to the total observed rate was on average  $37\%$ , which was close to the average ratio of coagulation loss to formation rate in urban Beijing,  $0.41$  (Yue et al., 2010), suggesting that coagulation loss was as important as  $dN_{\text{nuc}}/dt$ . The formation rate ( $J_{\text{D}}$ ) ranged from  $0.2$  to  $16.2\text{ cm}^{-3}\text{ s}^{-1}$  in urban Lanzhou, which was lower than the observations at some urban sites, such as in Beijing,  $3.3\text{--}81.4\text{ cm}^{-3}\text{ s}^{-1}$  (Wu et al., 2007), and St. Louis, with a mean value of  $17.0\text{ cm}^{-3}\text{ s}^{-1}$  (Qian et al., 2007), but much higher

than in regional nucleation episodes ( $0.01\text{--}10\text{ cm}^{-3}\text{ s}^{-1}$ ) at most other sites (Kulmala et al., 2004).

Compared to  $J_{\text{D}}$ , GR varied less in inter-annual scale and ranged from  $0.5$  to  $14.9\text{ nm h}^{-1}$ , which is slightly higher than that in urban Beijing,  $0.3\text{--}11.2\text{ nm h}^{-1}$  (Wu et al., 2007), and also within the range of the typical particle growth rate of  $1\text{--}20\text{ nm h}^{-1}$  in mid-latitudes (Kulmala et al., 2004). The mean CS values were between  $0$  and  $0.01\text{ s}^{-1}$  with less fluctuation during the campaign (Fig. 11f). Shen et al. (2011) found that the mean value of CS was  $0.02\text{ s}^{-1}$  during NPF events in the North China Plain, which was much higher than our results. Therefore, NPF events were less impacted by the condensation sink during our campaign. The less-varied  $N_{100-800}$  during 2015–2019 compared to that during 2012–2014 may be related to the condensation of low-volatility vapors, which resulted in a relatively high condensation sink (Fig. 11j). Based on the method presented in Dada et al. (2020), we also calculated the  $\text{H}_2\text{SO}_4$  proxy to estimate the changes in the NPF precursors over the study period (Fig. 11g). The  $\text{H}_2\text{SO}_4$  proxy varied from  $3.3 \times 10^7$  to  $6.0 \times 10^8\text{ cm}^{-3}$ , with average concentration of  $2.5 \times 10^8\text{ cm}^{-3}$  over the study period, which was slightly higher than that in urban Beijing (Dada et al., 2020) due to more coal combustion and basin terrain in urban Lanzhou.

### 3.5 Role of meteorology and air masses

NPF events predominantly occurred under dry and sunny weather conditions (Birmili and Wiedensohler, 2000; Kerminen et al., 2018). According to a relatively recent review on regional NPF in different environments of the global troposphere, the observed factors that favor the occurrence of

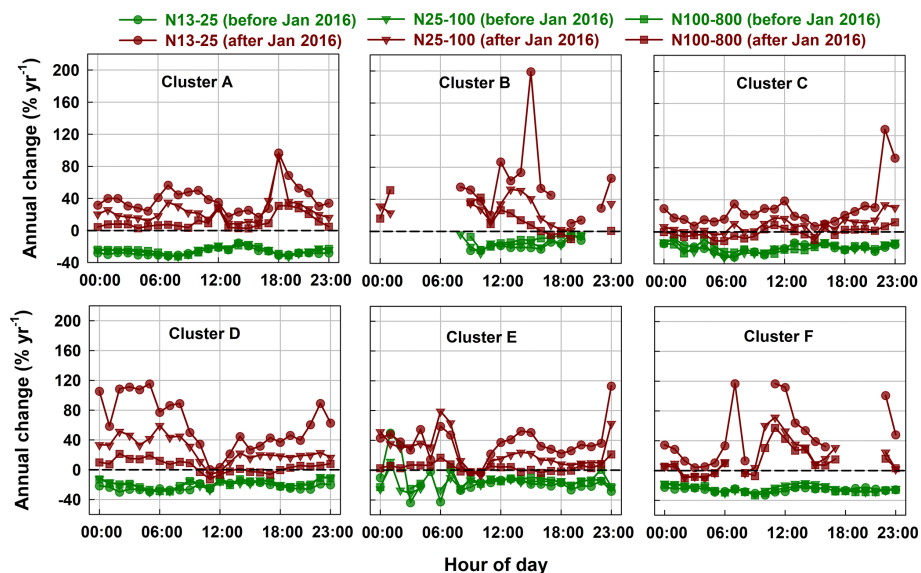


**Figure 10.** Diurnal variations in the trends of PNCs in three modes for the two contrasting periods (before vs. after January 2016) for each cluster. The annual change is calculated by Theil–Sen regression, and the calculation is shown in Sect. 2.4 (Trend analysis methods).

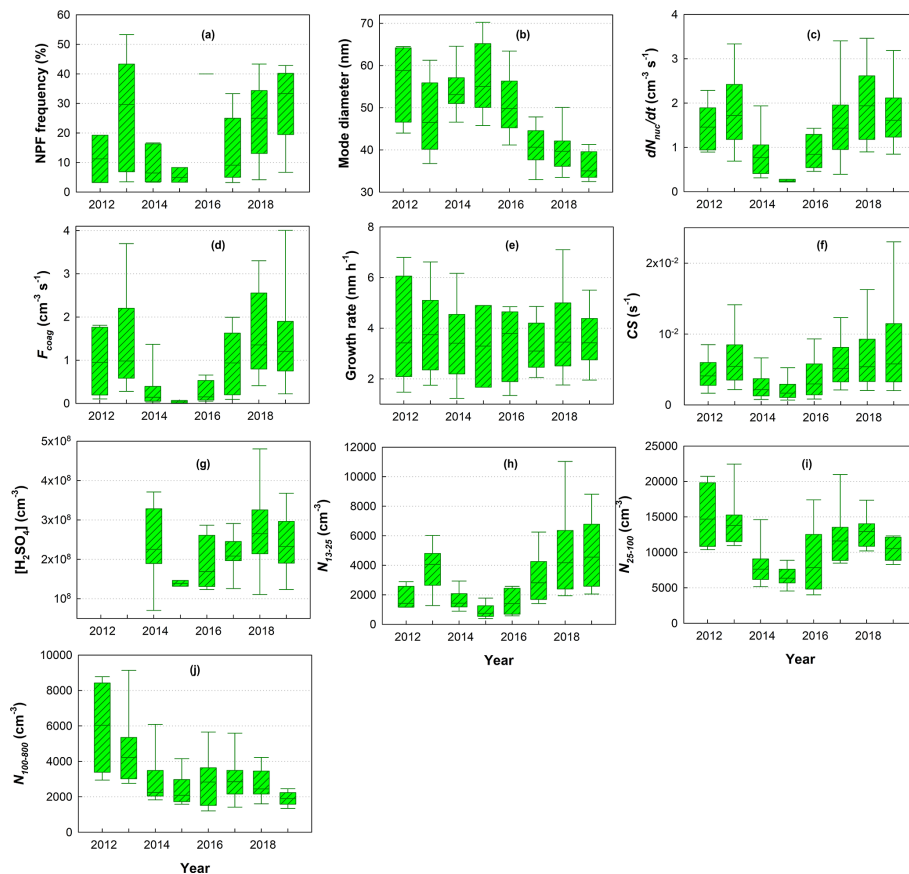


**Figure 11.** Inter-annual statistics of the trends of NPF frequency, mode diameter, formation ( $dN_{\text{nuc}}/dt$ ,  $F_{\text{coag}}$ ) and growth rates, CS and  $\text{H}_2\text{SO}_4$  proxy, and number concentrations in the three bins ( $N_{13-25}$ ,  $N_{25-100}$ ,  $N_{100-800}$ ) during the campaign. The lines inside the box denote the median slope; the two whiskers and the top and bottom of the box denote the 5th and 95th and the 75th and 25th percentiles.

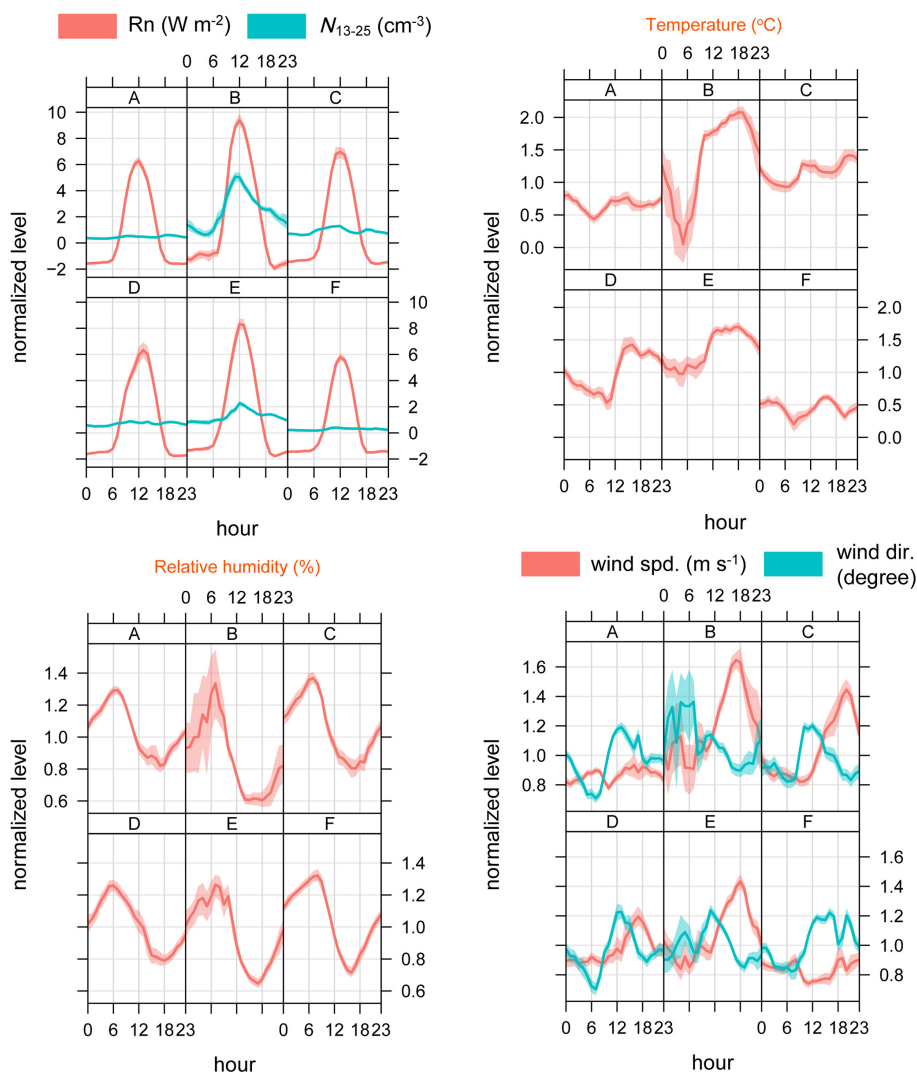


**Figure 12.** Normalized diurnal variations of net radiation ( $R_n$ ),  $N_{13-25}$ , temperature, relative humidity, and wind speed and direction for each cluster during the campaign. The shading shows the estimated 95 % confidence intervals.

regional NPF include a high intensity of solar radiation, low RH, high gas-phase sulfuric acid concentration and low pre-existing aerosol loading (Kerminen et al., 2018). Possible reasons for the apparently close connection between the ambient RH and occurrence of NPF have been proposed, including the typically negative feedback of high RH on the solar radiation intensity, photochemical reactions and atmospheric lifetime of aerosol precursor vapors. The effect of the ambient temperature ( $T$ ) on NPF shows very different responses between different studies, which is probably related to the simultaneous presence of several temperature-dependent processes that may either enhance or suppress NPF. Therefore, the meteorological parameters affect NPF process by modulating the condensation and coagulation sink. Figures 12 and S19 show the diurnal and inter-annual variations in meteorological parameters such as net radiation, temperature, relative humidity, and wind speed and direction for each cluster

during the campaign to better understand response of PNCs to meteorology. The peak of net radiation and  $N_{13-25}$  coincided at noon for NPF\_C, and their peaks were significantly higher than those for the other clusters (Fig. 12). The increased daylight net radiation for Cluster B could also partly explain the higher  $N_{13-25}$  induced by the more frequent NPF events after 2016, especially in spring (Figs. S19 and S20). The higher ambient temperature and lower relative humidity at noon and the larger daily ranges for NPF\_C also indicated that dry and hot air in a sunny day was conducive to forming new particles. In addition, NPF events corresponding to large southeasterly winds may be because accumulation mode particles were dispersed and diluted by strong winds and thus coagulation sink decreased, which can be supported by the above results. According to the empirically based mathematical function between number concentrations of fine particles (FPs, diameter < 2.5  $\mu\text{m}$ ) and meteorological variables, Hus-

sein et al. (2006) found that the predicted number concentrations of accumulation mode particles follow this relationship more closely than those of UFPs due to the origin and type of aerosol particles in the accumulation mode size range, being mainly regional and long-range transported. The main limitation of the mathematical function in their study was during NPF events, indicating that particles in nucleation and accumulation modes were differently dependent on meteorological variables.

A general finding was that changes in aerosol were related to air mass changes (Birmili et al., 2001), and dust aerosols from the Gobi Desert at the Hexi Corridor could be transported to Lanzhou and affect urban PM pollution (Zhao et al., 2015b). Figure S21 illustrates gridded back trajectory frequencies with hexagonal binning for each cluster to explore the impacts of air mass on variations of particle number. The huge discrepancy of back trajectory frequencies among the six clusters suggested that the air mass history has a significant impact on urban particle number concentrations and size distributions. For example, back trajectories were mainly from the adjacent regions of urban Lanzhou and were less affected by long-range transport for NPF\_C, and thus the particles were not easily grown by coagulation during transport processes, which was conducive to the occurrence of NPF events. In urban Beijing, Wang et al. (2013) also indicated that mean total PNCs from the northern directions were higher than the air masses that came from other directions, while more volume concentrations were observed for the air masses from the southwest and the south. Therefore, particle number size distributions in urban Lanzhou were partly affected by air mass conditions.

#### 4 Summary and conclusions

The first in situ observations of particle number size distributions (PNSDs) in the size range of 13–800 nm were conducted from 2012 to 2019 in urban Lanzhou, a typical valley city in western China. Meanwhile, the mass concentrations of the criteria air pollutants ( $\text{PM}_{2.5}$ ,  $\text{PM}_{10}$ ,  $\text{O}_3$ ,  $\text{SO}_2$ ,  $\text{NO}_2$ , and CO), AOD and meteorological variables (temperature, relative humidity, wind speed and direction, and net radiation) were also measured during the campaign. The customized Sen–Theil trend estimator and  $k$ -means clustering technique were used to explore the trends of PNCs and the criteria air pollutants, as well as to reveal the contributions of variations in primary emissions due to the clean air action plan and secondary formation to PNCs. Some novel findings were obtained as follows.

The mean values for particle number in nucleation ( $N_{13-25}$ ), Aitken ( $N_{25-100}$ ) and accumulation modes ( $N_{100-800}$ ) were respectively 2514.0, 10 768.7, and  $3258.4 \text{ cm}^{-3}$ , and  $N_{25-100}$  accounted for about 65.1 % of total PNCs during the campaign. The particle number in the three modes declined largely during 2012–2015; for

example, summer  $N_{13-25}$  decreased by around 75 % in 2015 compared to that in 2013. However,  $N_{13-25}$  increased significantly during 2016–2019, which was consistent with  $\text{O}_3$  while showing the opposite trend with declining  $\text{PM}_{2.5}$  during the period. The most obvious increase in  $N_{13-25}$  was during 12:00–16:00 in summer months, and the largest increase corresponded to easterly, southerly and southeasterly winds.  $N_{25-100}$  and  $N_{100-800}$  first increased during 2016–2017 and then decreased until 2019, and their variations were consistent with the primary emitted pollutants ( $\text{SO}_2$ ,  $\text{NO}_2$ ). The  $N_{25-100}$  difference between the two periods (2012–2015 vs. 2016–2019) was much less significant than  $N_{13-25}$ , and the most obvious  $N_{25-100}$  increase occurred in the morning and evening rush hours for northeasterly winds. In diurnal and annual cycles, the  $N_{100-800}$  and  $\text{PM}_{2.5}$  trends for the two periods were opposite to  $N_{13-25}$ , with a significant reduction at noon in the summer months for southerly winds, and thus the reduced coagulation sink was conducive to the occurrence of NPF events.

The  $k$ -means clustering technique was used to classify the hourly average PNSDs into six clusters during the measurement campaign. The shape and mode diameter of PNSDs were largely different among the clusters with varying mode diameters from  $\sim 20$  to 70 nm. According to the annual and diurnal variations of occurrence frequency, PNSD, the corresponding air pollutants and meteorological parameters, the sources and key influencing factors were determined for each cluster. The two most polluted clusters (A and F), Pollut\_C, were mainly affected by the primary emissions from human activities and poor diffusion conditions. Cluster B was followed by Cluster E, and  $N_{13-25}$  had a sharp peak in the afternoon in the warm months, and thus the two clusters represented new particle formation and growth event impacts. Cluster C suggested an urban background PNSD, while Cluster D was jointly affected by motor vehicle emissions and NPF events. The response of particle number to air pollution control was largely different for each size fraction, which may be closely related to the variations in coagulation sink and meteorological conditions induced by reduced primary emissions. Based on trends of daily mean particle number in the three modes as wind directions for each cluster, the contributions of primary emissions and secondary formation to PNCs were evaluated in this study. The southeasterly winds corresponded to more  $\text{PM}_{2.5}$  reduction on summer afternoons in response to emission control policies, and thus more solar radiation reached the ground surface, which promoted NPF occurrence due to the reduced coagulation sink. The polluted clusters governed the winter PNCs before 2016, and their occurrence was less and less frequent after 2016, which was largely dominated by the reduction in primary emissions. However, the contribution of NPF events to summer  $N_{13-25}$  decreased from 50 % to about 10 % during 2013 to 2015 and then increased to reach around 60 % in 2019.

Theil–Sen regression was used to quantitatively evaluate the changing trends of size-resolved PNCs, and they exhib-

ited downward trends for all clusters during 2012–2015, especially in spring. The annual relative slopes of spring PNCs varied from  $-54.7\%$  for Cluster F to  $-17.2\%$  for Cluster B, from  $-42.6\%$  for Cluster A to  $-14.1\%$  for Cluster B, and from  $-40.7\%$  for Cluster A to  $-17.5\%$  for Cluster B per year for the 13–25, 25–100, and 100–800 nm size ranges. The UFPs number was increased, and the amplitude was greater during 2016–2019. The annual relative slopes of  $N_{13-25}$  varied between  $5.1\%$  (fall) and  $314.4\%$  (winter), between  $8.0$  (fall) and  $135.5\%$  (spring), between  $11.3\%$  (fall) and  $184.3\%$  (winter), between  $-4.5$  (fall) and  $59.1\%$  (summer), between  $6.3\%$  (fall) and  $30.3\%$  (spring), and between  $3.6\%$  (fall) and  $15.7\%$  (spring) for clusters A–F. The increased daytime net radiation, higher ambient temperature and lower relative humidity at noon for NPF events also could partly explain the higher  $N_{13-25}$  induced by the more frequent nucleation events after 2016, especially in spring. The air mass history had a significant impact on urban PNSDs. The back trajectories were mainly from the adjacent regions of urban Lanzhou and less affected by long-range transport for NPF events, and thus the particles were not easily grown by coagulation during transport processes, which was helpful for the occurrence of NPF events. In this study, the measurement campaign was conducted at a Chinese cities in western China, but the similar PNCs trends and influencing factors should be expected in other Chinese cities. In future work, we will establish the PNSD observation network in some megacities to better evaluate the response of PNCs to emission mitigation policies in China.

*Code and data availability.* The data used and the code for processing the data in this work can be obtained by contacting the corresponding author (zhaosp@lzb.ac.cn).

*Supplement.* The supplement related to this article is available online at: <https://doi.org/10.5194/acp-21-14959-2021-supplement>.

*Author contributions.* SZ and YY designed the study. SZ analyzed the data with help from YY and DQ. DY and LD collected and analyzed the particle number size distributions and meteorology data during the campaign. JL conducted the field experiment.

*Competing interests.* The contact author has declared that neither they nor their co-authors have any competing interests

*Disclaimer.* Publisher's note: Copernicus Publications remains neutral with regard to jurisdictional claims in published maps and institutional affiliations.

*Acknowledgements.* We thank Longxiang Dong, Jin Xie and Chenchen Ma for their contributions to the experiment. We thank the editor and two anonymous referees for their suggestions, which improved the paper.

*Financial support.* This research has been supported by the National Natural Science Foundation of China (grant nos. 42075185 and 41605103), the Youth Innovation Promotion Association of the Chinese Academy of Sciences (grant no. 2017462), and the Gansu Science and Technology Program key projects (grant nos. 20JR10RA037 and 18JR2RA005), the CPSF-CAS Joint Foundation for Excellent Postdoctoral Fellows (2016LH0020).

*Review statement.* This paper was edited by Veli-Matti Kerminen and reviewed by two anonymous referees.

## References

- Andreae, M. O. and Rosenfeld, D.: Aerosol-cloud-precipitation interactions, Part 1. The nature and sources of cloud-active aerosols, *Earth-Sci. Rev.*, 89, 13–41, <https://doi.org/10.1016/j.earscirev.2008.03.001>, 2008.
- Asmi, A., Wiedensohler, A., Laj, P., Fjaeraa, A.-M., Sellegri, K., Birmili, W., Weingartner, E., Baltensperger, U., Zdimal, V., Zikova, N., Putaud, J.-P., Marinoni, A., Tunved, P., Hansson, H.-C., Fiebig, M., Kivekäs, N., Lihavainen, H., Asmi, E., Ulevicius, V., Aalto, P. P., Swietlicki, E., Kristensson, A., Mihalopoulos, N., Kalivitis, N., Kalapov, I., Kiss, G., de Leeuw, G., Henzing, B., Harrison, R. M., Beddows, D., O'Dowd, C., Jennings, S. G., Flentje, H., Weinhold, K., Meinhardt, F., Ries, L., and Kulmala, M.: Number size distributions and seasonality of submicron particles in Europe 2008–2009, *Atmos. Chem. Phys.*, 11, 5505–5538, <https://doi.org/10.5194/acp-11-5505-2011>, 2011.
- Asmi, A., Collaud Coen, M., Ogren, J. A., Andrews, E., Sheridan, P., Jefferson, A., Weingartner, E., Baltensperger, U., Bukowiecki, N., Lihavainen, H., Kivekäs, N., Asmi, E., Aalto, P. P., Kulmala, M., Wiedensohler, A., Birmili, W., Hamed, A., O'Dowd, C., G Jennings, S., Weller, R., Flentje, H., Fjaeraa, A. M., Fiebig, M., Myhre, C. L., Hallar, A. G., Swietlicki, E., Kristensson, A., and Laj, P.: Aerosol decadal trends – Part 2: In-situ aerosol particle number concentrations at GAW and ACTRIS stations, *Atmos. Chem. Phys.*, 13, 895–916, <https://doi.org/10.5194/acp-13-895-2013>, 2013.
- Birmili, W. and Wiedensohler, A.: New particle formation in the continental boundary layer: Meteorological and gas phase parameter influence, *Geophys. Res. Lett.*, 27, 3325–3328, 2000.
- Birmili, W., Wiedensohler, A., Heintzenberg, J., and Lehmann, K.: Atmospheric particle number size distribution in central Europe: Statistical relations to air mass and meteorology, *J. Geophys. Res.*, 32, 5–18, 2001.
- Birmili, W., Heinke, K., Pitz, M., Matschullat, J., Wiedensohler, A., Cyrys, J., Wichmann, H.-E., and Peters, A.: Particle number size distributions in urban air before and after volatilisation, *Atmos. Chem. Phys.*, 10, 4643–4660, <https://doi.org/10.5194/acp-10-4643-2010>, 2010.

- Birmili, W., Weinhold, K., Rasch, F., Sonntag, A., Sun, J., Merkel, M., Wiedensohler, A., Bastian, S., Schladitz, A., Löschau, G., Cyrys, J., Pitz, M., Gu, J., Kusch, T., Flentje, H., Quass, U., Kaminski, H., Kuhlbusch, T. A. J., Meinhardt, F., Schwerin, A., Bath, O., Ries, L., Gerwig, H., Wirtz, K., and Fiebig, M.: Long-term observations of tropospheric particle number size distributions and equivalent black carbon mass concentrations in the German Ultrafine Aerosol Network (GUAN), *Earth Syst. Sci. Data*, 8, 355–382, <https://doi.org/10.5194/essd-8-355-2016>, 2016.
- Bodhaine, B. A.: Aerosol measurements at four background sites, *J. Geophys. Res.*, 88, 10753–10768, <https://doi.org/10.1029/JC088iC15p10753>, 1983.
- Boy, M. and Kulmala, M.: Nucleation events in the continental boundary layer: Influence of physical and meteorological parameters, *Atmos. Chem. Phys.*, 2, 1–16, <https://doi.org/10.5194/acp-2-1-2002>, 2002.
- Chen, C. H., Huang, J. G., Ren, Z. H., and Peng, X. A.: Meteorological conditions of photochemical smog pollution during summer in Xigu industrial area, *Acta Sci. Circumst.*, 6, 334–342, 1986 (in Chinese).
- Chen, C., Sun, Y. L., Xu, W. Q., Du, W., Zhou, L. B., Han, T. T., Wang, Q. Q., Fu, P. Q., Wang, Z. F., Gao, Z. Q., Zhang, Q., and Worsnop, D. R.: Characteristics and sources of submicron aerosols above the urban canopy (260 m) in Beijing, China, during the 2014 APEC summit, *Atmos. Chem. Phys.*, 15, 12879–12895, <https://doi.org/10.5194/acp-15-12879-2015>, 2015.
- Chu, P. C., Chen, Y. C., Lu, S. H., Li, Z. C., and Lu Y. Q.: Particulate air pollution in Lanzhou China, *Environ. Int.*, 34, 698–713, 2008.
- Cusack, M., Pérez, N., Pey, J., Alastuey, A., and Querol, X.: Source apportionment of fine PM and sub-micron particle number concentrations at a regional background site in the western Mediterranean: a 2.5 year study, *Atmos. Chem. Phys.*, 13, 5173–5187, <https://doi.org/10.5194/acp-13-5173-2013>, 2013.
- Dada, L., Yliviikka, I., Baalbaki, R., Li, C., Guo, Y., Yan, C., Yao, L., Sarnela, N., Jokinen, T., Daellenbach, K. R., Yin, R., Deng, C., Chu, B., Nieminen, T., Wang, Y., Lin, Z., Thakur, R. C., Kontkanen, J., Stolzenburg, D., Sipilä, M., Hussein, T., Paasonen, P., Bianchi, F., Salma, I., Weidinger, T., Pikridas, M., Sciare, J., Jiang, J., Liu, Y., Petäjä, T., Kerminen, V.-M., and Kulmala, M.: Sources and sinks driving sulfuric acid concentrations in contrasting environments: implications on proxy calculations, *Atmos. Chem. Phys.*, 20, 11747–11766, <https://doi.org/10.5194/acp-20-11747-2020>, 2020.
- Dal Maso, M., Kulmala, M., Riipinen, I., Wagner, R., Hussein, T., Aalto, P. P., and Lehtinen, K. E. J.: Formation and growth of fresh atmospheric aerosols: eight years of aerosol size distribution data from SMEAR II, Hyytiälä, Finland, *Boreal Environ. Res.*, 10, 323–336, 2005.
- Dal Maso, M., Hyvärinen, A., Komppula, M., Tunved, P., Kerminen, V.-M., Lihavainen, H., Öviisanen, Y., Hansson, H.-C., and Kulmala, M.: Annual and interannual variation in boreal forest aerosol particle number and volume concentration and their connection to particle formation, *Tellus B*, 60, 495–508, 2008.
- Dinoli, A., Weinhold, K., Wiedensohler, A., and Contini, D.: Study of new particle formation events in southern Italy, *Atmos. Environ.*, 244, 117920, <https://doi.org/10.1016/j.atmosenv.2020.117920>, 2021.
- Fuchs, N. A.: *The mechanics of aerosols*, Pergamon, Pp, xiv, 408, 1964.
- Gani, S., Bhandari, S., Patel, K., Seraj, S., Soni, P., Arub, Z., Habib, G., Hildebrandt Ruiz, L., and Apte, J. S.: Particle number concentrations and size distribution in a polluted megacity: the Delhi Aerosol Supersite study, *Atmos. Chem. Phys.*, 20, 8533–8549, <https://doi.org/10.5194/acp-20-8533-2020>, 2020.
- Gao, Y., Zhang, M., Liu, Z., Wang, L., Wang, P., Xia, X., Tao, M., and Zhu, L.: Modeling the feedback between aerosol and meteorological variables in the atmospheric boundary layer during a severe fog–haze event over the North China Plain, *Atmos. Chem. Phys.*, 15, 4279–4295, <https://doi.org/10.5194/acp-15-4279-2015>, 2015.
- Guo, S., Hu, M., Zamora, M. L., Peng, J., Shang, D., Zheng, J., Du, Z., Wu, Z., Shao, M., Zeng, L., Molina, M. J., and Zhang, R. Y.: Elucidating severe urban haze formation in China, *P. Natl. Acad. Sci. USA*, 111, 17373–17378, <https://doi.org/10.1073/pnas.1419604111>, 2014.
- Heintzenberg, J., Birmili, W., Otto, R., Andreae, M. O., Mayer, J.-C., Chi, X., and Panov, A.: Aerosol particle number size distributions and particulate light absorption at the ZOTTO tall tower (Siberia), 2006–2009, *Atmos. Chem. Phys.*, 11, 8703–8719, <https://doi.org/10.5194/acp-11-8703-2011>, 2011.
- Hu, J., Huang, L., Chen, M., Liao, H., Zhang, H., Wang, S., Zhang Q., and Ying, Q.: Premature mortality attributable to particulate matter in China: source contributions and responses to reductions, *Environ. Sci. Tech.*, 51, 9950–9959, 2017.
- Hussein, T., Puustinen, A., Aalto, P. P., Mäkelä, J. M., Hämeri, K., and Kulmala, M.: Urban aerosol number size distributions, *Atmos. Chem. Phys.*, 4, 391–411, <https://doi.org/10.5194/acp-4-391-2004>, 2004.
- Hussein, T., Karppinen, A., Kukkonen, J., Harkonen, J., Aalto, P. P., Hämeri, K., Kerminen, V.-M., and Kulmala, M.: Meteorological dependence of size-fractionated number concentrations of urban aerosol particles, *Atmos. Environ.*, 40, 1427–1440, 2006.
- Kanawade, V. P., Tripathi, S. N., Bhattu, D., and Shamjad, P. M.: Sub-micron particle number size distributions characteristics at an urban location, Kanpur, in the Indo-Gangetic Plain, *Atmos. Res.*, 147, 121–132, 2014.
- Kerminen, V.-M., Chen, X., Vakkari, V., Petäjä, T., Kulmala, M., and Bianchi, F.: Atmospheric new particle formation and growth: review of field observations, *Environ. Res. Lett.*, 13, 103003, <https://doi.org/10.1088/1748-9326/aadf3c>, 2018.
- Kivekäs, N., Sun, J., Zhan, M., Kerminen, V.-M., Hyvärinen, A., Komppula, M., Viisanen, Y., Hong, N., Zhang, Y., Kulmala, M., Zhang, X.-C., Deli-Geer, and Lihavainen, H.: Long term particle size distribution measurements at Mount Waliguan, a high-altitude site in inland China, *Atmos. Chem. Phys.*, 9, 5461–5474, <https://doi.org/10.5194/acp-9-5461-2009>, 2009.
- Krecl, P., Johansson, C., Targino, A. C., Strom, J., and Burman, L.: Trends in black carbon and size-resolved particle number concentrations and vehicle emission factors under real-world conditions, *Atmos. Environ.*, 165, 155–168, 2017.
- Kulmala, M.: How particles nucleate and grow, *Science*, 302, 1000–1001, 2003.
- Kulmala, M., Vehkamäki, H., Petäjä, T., Dal Maso, M., Lauri, A., Kerminen, V. M., Birmili, W., and McMurry, P. H.: Formation and growth rates of ultrafine atmospheric particles: a review of observations, *J. Aerosol Sci.*, 35, 143–176, 2004.
- Kulmala, M., Petaja, T., Nieminen, T., Sipilä, M., Manninen, H. E., Lehtipalo, K., Dal Maso, M., Aalto, P. P., Junninen, H., Paa-

- sonen, P., Riipinen, I., Lehtinen, K. E. J., Laaksonen, A., and Kerminen, V. M.: Measurement of the nucleation of atmospheric aerosol particles, *Nat. Protoc.*, 7, 1651–1667, 2012.
- Kulmala, M., Dada, L., Daellenbach, K. R., Yan, C., Stolzenburg, D., Kontkanen, J., Ezhova, E., Hakala, S., Tuovinen, S., Kokkonen, T. V., Kurppa, M., Cai, R. L., Zhou, Y., Yin, R., Baalbaki, R., Chan, T., Chu, B., Deng, C., Fu, Y., Ge, M. F., He, H., Heikkinen, L., Junninen, H., Liu, Y., Lu, Y., Nie, W., Rusanen, A., Vakkari, V., Wang, Y., Yang, G., Yao, L., Zheng, J., Kujansuu, J., Kangasluoma, J., Petaja, T., Paasonen, P., Jarvi, L., Worsnop, D., Ding, A. J., Liu, Y., Wang, L., Jiang, J. K., Bianchi, F., and Kerminen, V.-M.: Is reducing new particle formation a plausible solution to mitigate particulate air pollution in Beijing and other Chinese megacities?, *Faraday Discuss.*, 226, 334–347, <https://doi.org/10.1039/d0fd00078g>, 2021.
- Lelieveld, J., Evans, J. S., Fnais, M., Giannadaki, D., and Pozzer, A.: The contribution of outdoor air pollution sources to premature mortality on a global scale, *Nature*, 525, 367, <https://doi.org/10.1038/nature15371>, 2015.
- Leoni, C., Pokorna, P., Hovorka, J., Masiol, M., Topinka, J., Zhao, Y. J., Krupal, K., Cliff, S., Mikuska, P., and Hopke, P. K.: Source apportionment of aerosol particles at a European air pollution hot spot using particle number size distributions and chemical composition, *Environ. Pollut.*, 234, 145–154, 2018.
- Li, J., Gao, W., Cao, L., Xiao, Y., Zhang, Y., Zhao, S., Liu, Z., Liu, Z., Tang, G., Ji, D., Hu, B., Song, T., He, L., Hu, M., and Wang, Y. S.: Significant changes in autumn and winter aerosol composition and sources in Beijing from 2012 to 2018: Effects of clean air actions, *Environ. Pollut.*, 268, 115855, <https://doi.org/10.1016/j.envpol.2020.115855>, 2021.
- Li, Z., Rosenfeld, D., and Fan, J.: Aerosols and their impact on radiation, clouds, precipitation, and severe weather events, *Oxford Research Encyclopedias*, Oxford University Press, Oxford, USA, <https://doi.org/10.1093/acrefore/9780199389414.013.126>, 2017.
- Liu, H., Pan, X. L., Wu, Y., Ji, D. S., Tian, Y., Chen, X. S., and Wang, Z. F.: Size-resolved mixing state and optical properties of black carbon at an urban site in Beijing, *Sci. Total Environ.*, 749, 141523, <https://doi.org/10.1016/j.scitotenv.2020.141523>, 2020.
- Ma, N. and Birmili, W.: Estimating the contribution of photochemical particle formation to ultrafine particle number averages in an urban atmosphere, *Sci. Total Environ.*, 512, 154–166, 2015.
- Makela, J. M., Aalto, P., Jokinen, V., Pohja, T., Nissinen, A., Palmroth, S., Markkanen, T., Seitsonen, K., Lihavainen, H., and Kulmala, M.: Observations of ultrafine aerosol particle formation and growth in boreal forest, *Geophys. Res. Lett.*, 24, 1219–1222, 1997.
- Oberdörster, G., Oberdörster, E., and Oberdörster, J.: Nanotoxicology: An emerging discipline evolving from studies of ultrafine particles, *Environ. Health Perspec.*, 113, 823–839, 2005.
- Pandolfi, M., Querol, X., Alastuey, A., Jimenez, J. L., Jorba, O., Day, D., Ortega, A., Cubison, M. J., Comerón, A., Sicard, M., Mohr, C., Prévôt, A. S. H., Minguillón, M. C., Pey, J., Baldasano, J. M., Burkhardt, J. F., Seco, R., Peñuelas, J., van Drooge, B. L., Artíñano, B., Di Marco, C., Nemitz, E., Schallhart, S., Metzger, A., Hansel, A., Lorente, J., Ng, S., Jayne, J., and Szidat, S.: Effects of sources and meteorology on particulate matter in the Western Mediterranean Basin: An overview of the DAURE campaign, *J. Geophys. Res.-Atmos.*, 119, 4978–5010, 2014.
- Qian, S., Sakurai, H., and McMurry, P. H.: Characteristics of regional nucleation events in urban East St. Louis, *Atmos. Environ.*, 41, 4119–4127, 2007.
- Rose, C., Collaud Coen, M., Andrews, E., Lin, Y., Bossert, I., Lund Myhre, C., Tuch, T., Wiedensohler, A., Fiebig, M., Aalto, P., Alastuey, A., Alonso-Blanco, E., Andrade, M., Artíñano, B., Arsov, T., Baltensperger, U., Bastian, S., Bath, O., Beukes, J. P., Brem, B. T., Bukowiecki, N., Casquero-Vera, J. A., Conil, S., Eleftheriadis, K., Favez, O., Flentje, H., Gini, M. I., Gómez-Moreno, F. J., Gysel-Beer, M., Hallar, A. G., Kalapov, I., Kalivitis, N., Kasper-Giebl, A., Keywood, M., Kim, J. E., Kim, S.-W., Kristensson, A., Kulmala, M., Lihavainen, H., Lin, N.-H., Lyamani, H., Marinoni, A., Martins Dos Santos, S., Mayol-Bracero, O. L., Meinhardt, F., Merkel, M., Metzger, J.-M., Mihalopoulos, N., Ondracek, J., Pandolfi, M., Pérez, N., Petäjä, T., Petit, J.-E., Picard, D., Pichon, J.-M., Pont, V., Putaud, J.-P., Reisen, F., Sellegri, K., Sharma, S., Schauer, G., Sheridan, P., Sherman, J. P., Schwerin, A., Sohmer, R., Sorribas, M., Sun, J., Tulet, P., Vakkari, V., van Zyl, P. G., Velarde, F., Villani, P., Vratolis, S., Wagner, Z., Wang, S.-H., Weinhold, K., Weller, R., Yela, M., Zdimal, V., and Laj, P.: Seasonality of the particle number concentration and size distribution: a global analysis retrieved from the network of Global Atmosphere Watch (GAW) near-surface observatories, *Atmos. Chem. Phys. Discuss.* [preprint], <https://doi.org/10.5194/acp-2020-1311>, in review, 2021.
- Sabaliauskas, K., Jeong, C.-H., Yao, X., Jun, Y.-S., and Evans, G.: Cluster analysis of roadside ultrafine particle size distributions, *Atmos. Environ.*, 70, 64–74, 2013.
- Schmale, J., Henning, S., Decesari, S., Henzing, B., Keskinen, H., Sellegri, K., Ovadnevaite, J., Pöhlker, M. L., Brito, J., Bougiatioti, A., Kristensson, A., Kalivitis, N., Stavroulas, I., Carbone, S., Jefferson, A., Park, M., Schlag, P., Iwamoto, Y., Aalto, P., Äijälä, M., Bukowiecki, N., Ehn, M., Frank, G., Fröhlich, R., Frumau, A., Herrmann, E., Herrmann, H., Holzinger, R., Kos, G., Kulmala, M., Mihalopoulos, N., Nenes, A., O’Dowd, C., Petäjä, T., Picard, D., Pöhlker, C., Pöschl, U., Poulain, L., Prévôt, A. S. H., Swietlicki, E., Andreae, M. O., Artaxo, P., Wiedensohler, A., Ogren, J., Matsuki, A., Yum, S. S., Stratmann, F., Baltensperger, U., and Gysel, M.: Long-term cloud condensation nuclei number concentration, particle number size distribution and chemical composition measurements at regionally representative observatories, *Atmos. Chem. Phys.*, 18, 2853–2881, <https://doi.org/10.5194/acp-18-2853-2018>, 2018.
- Schmid, O. and Stoeger, T.: Surface area is the biologically most effective dose metric for acute nanoparticle toxicity in the lung, *J. Aerosol Sci.*, 99, 133–143, 2016.
- Seinfeld, J. H. and Pandis, S. N.: *Atmospheric chemistry and physics of air pollution*, John Wiley and Sons, Inc., New York, USA, 2006.
- Shen, X. J., Sun, J. Y., Zhang, Y. M., Wehner, B., Nowak, A., Tuch, T., Zhang, X. C., Wang, T. T., Zhou, H. G., Zhang, X. L., Dong, F., Birmili, W., and Wiedensohler, A.: First long-term study of particle number size distributions and new particle formation events of regional aerosol in the North China Plain, *Atmos. Chem. Phys.*, 11, 1565–1580, <https://doi.org/10.5194/acp-11-1565-2011>, 2011.
- Shen, X. J., Sun, J. Y., Zhang, X. Y., Zhang, Y. M., Zhang, L., Fan, R. X., Zhang, Z. X., Zhang, X. L., Zhou, H. G., Zhou, L. Y., Dong, F., and Shi, Q. F.: The influence of emission control on

- particle number size distribution and new particle formation during China's V-Day parade in 2015, *Sci. Total Environ.*, 573, 409–419, <https://doi.org/10.1016/j.scitotenv.2016.08.085>, 2016.
- Shi, H. R., Zhang, J. Q., Zhao, B., Xia, X. A., Hu, B., Chen, H. B., Wei, J., Liu, M. Q., Bian, Y. X., Fu, D. S., Gu, Y., and Liou, K.-N.: Surface Brightening in Eastern and Central China Since the Implementation of the Clean Air Action in 2013: Causes and Implications, *Geophys. Res. Lett.*, 48, e2020GL091105, <https://doi.org/10.1029/2020GL091105>, 2021.
- Stanier, C. O., Khlystov, A. Y., and Pandis, S. N.: Ambient aerosol size distributions and number concentrations measured during the Pittsburgh Air Quality Study (PAQS), *Atmos. Environ.*, 38, 275–3284, 2004.
- Sun, J., Birmili, W., Hermann, M., Tuch, T., Weinhold, K., Merkel, M., Rasch, F., Müller, T., Schladitz, A., Bastian, S., Löschau, G., Cyrys, J., Gu, J., Flentje, H., Briel, B., Asbach, C., Kaminski, H., Ries, L., Sohmer, R., Gerwig, H., Wirtz, K., Meinhardt, F., Schwerin, A., Bath, O., Ma, N., and Wiedensohler, A.: Decreasing trends of particle number and black carbon mass concentrations at 16 observational sites in Germany from 2009 to 2018, *Atmos. Chem. Phys.*, 20, 7049–7068, <https://doi.org/10.5194/acp-20-7049-2020>, 2020.
- Tunved, P., Ström, J., and Hansson, H.-C.: An investigation of processes controlling the evolution of the boundary layer aerosol size distribution properties at the Swedish background station Aspvreten, *Atmos. Chem. Phys.*, 4, 2581–2592, <https://doi.org/10.5194/acp-4-2581-2004>, 2004.
- von Bismarck-Osten, C., Birmili, W., Ketzler, M., Massling, A., Petäjä, T., and Weber, S.: Characterization of parameters influencing the spatio-temporal variability of urban particle number size distributions in four European cities, *Atmos. Environ.*, 77, 415–429, 2013.
- Vu, T. V., Delgado-Saborit, J. M., and Harrison, R. M.: Review: Particle number size distributions from seven major sources and implications for source apportionment studies, *Atmos. Environ.*, 122, 114–132, 2015.
- Wang, Y., Hopke, P. K., Chalupa, D. C., and Utell, M. J.: Long-term study of urban ultrafine particles and other pollutants, *Atmos. Environ.*, 45, 7672–7680, 2011.
- Wang, Z. B., Hu, M., Wu, Z. J., Yue, D. L., He, L. Y., Huang, X. F., Liu, X. G., and Wiedensohler, A.: Long-term measurements of particle number size distributions and the relationships with air mass history and source apportionment in the summer of Beijing, *Atmos. Chem. Phys.*, 13, 10159–10170, <https://doi.org/10.5194/acp-13-10159-2013>, 2013.
- Wehner, B., Wiedensohler, A., Tuch, T. M., Wu, Z. J., Hu, M., Slanina, J., and Kiang, C. S.: Variability of the aerosol number size distribution in Beijing, China: New particle formation, dust storms, and high continental background, *Geophys. Res. Lett.*, 31, L22108, <https://doi.org/10.1029/2004GL021596>, 2004.
- Wehner, B., Birmili, W., Ditas, F., Wu, Z., Hu, M., Liu, X., Mao, J., Sugimoto, N., and Wiedensohler, A.: Relationships between submicrometer particulate air pollution and air mass history in Beijing, China, 2004–2006, *Atmos. Chem. Phys.*, 8, 6155–6168, <https://doi.org/10.5194/acp-8-6155-2008>, 2008.
- WHO: Air quality guidelines for Europe, 2nd Edn., Copenhagen, World Health Organization Regional Office for Europe, WHO Regional Publications, European Series No. 91, 2000.
- World Health Organization (WHO), Ambient Air Quality Database, available at: <https://whoairquality.shinyapps.io/AmbientAirQualityDatabase/> (last access: 5 July 2014), 2018.
- Wiedensohler, A., Birmili, W., Nowak, A., Sonntag, A., Weinhold, K., Merkel, M., Wehner, B., Tuch, T., Pfeifer, S., Fiebig, M., Fjåraa, A. M., Asmi, E., Sellegri, K., Depuy, R., Venzac, H., Villani, P., Laj, P., Aalto, P., Ogren, J. A., Swietlicki, E., Williams, P., Roldin, P., Quincey, P., Hüglin, C., Fierz-Schmidhauser, R., Gysel, M., Weingartner, E., Riccobono, F., Santos, S., Grünig, C., Faloon, K., Beddows, D., Harrison, R., Monahan, C., Jennings, S. G., O'Dowd, C. D., Marinoni, A., Horn, H.-G., Keck, L., Jiang, J., Scheckman, J., McMurry, P. H., Deng, Z., Zhao, C. S., Moerman, M., Henzing, B., de Leeuw, G., Löschau, G., and Bastian, S.: Mobility particle size spectrometers: harmonization of technical standards and data structure to facilitate high quality long-term observations of atmospheric particle number size distributions, *Atmos. Meas. Tech.*, 5, 657–685, <https://doi.org/10.5194/amt-5-657-2012>, 2012.
- Wu, Z. J., Hu, M., Liu, S., Wehner, B., Bauer, S., Blling, A. M., Wiedensohler, A., Petäjä, T., Dal Maso, M., and Kulmala, M.: New particle formation in Beijing, China: Statistical analysis of a 1-year data set, *J. Geophys. Res.*, 112, D09209, <https://doi.org/10.1029/2006JD007406>, 2007.
- Wu, Z. J., Hu, M., Lin, P., Liu, S., Wehner, B., and Wiedensohler, A.: Particle number size distribution in the urban atmosphere of Beijing, China, *Atmos. Environ.*, 42, 7967–7980, 2008.
- Yue, D. L., Hu, M., Zhang, R. Y., Wang, Z. B., Zheng, J., Wu, Z. J., Wiedensohler, A., He, L. Y., Huang, X. F., and Zhu, T.: The roles of sulfuric acid in new particle formation and growth in the mega-city of Beijing, *Atmos. Chem. Phys.*, 10, 4953–4960, <https://doi.org/10.5194/acp-10-4953-2010>, 2010.
- Zhai, S., Jacob, D. J., Wang, X., Shen, L., Li, K., Zhang, Y., Gui, K., Zhao, T., and Liao, H.: Fine particulate matter (PM<sub>2.5</sub>) trends in China, 2013–2018: separating contributions from anthropogenic emissions and meteorology, *Atmos. Chem. Phys.*, 19, 11031–11041, <https://doi.org/10.5194/acp-19-11031-2019>, 2019.
- Zhao, H. J., Gui, K., Ma, Y. J., Wang, Y. F., Wang, Y. Q., Wang, H., Zheng, Y., Li, L., Zhang, L., Che, H. Z., and Zhang, X. Y.: Climatology and trends of aerosol optical depth with different particle size and shape in northeast China from 2001 to 2018, *Sci. Total Environ.*, 763, 142979, <https://doi.org/10.1016/j.scitotenv.2020.142979>, 2021.
- Zhao, S. P., Yu, Y., and Qin, D. H.: From highly polluted inland city of China to “Lanzhou Blue”: The air-pollution characteristics, *Sciences in Cold and Arid Regions*, 10, 12–26, 2018.
- Zhao, S. P., Yu, Y., Yin, D. Y., and He, J. J.: Meteorological dependence of particle number concentrations in an urban area of complex terrain, Northwestern China, *Atmos. Res.*, 164, 304–317, 2015a.
- Zhao, S. P., Yu, Y., Xia, D. S., Yin, D. Y., He, J. J., Liu, N., and Li, F.: Urban particle size distributions during two contrasting dust events originating from Taklimakan and Gobi Deserts, *Environ. Pollut.*, 207, 107–122, 2015b.
- Zhao, S. P., Yu, Y., Yin, D. Y., He, J. J., Liu, N., Qu, J. J., and Xiao, J. H.: Annual and diurnal variations of gaseous and particulate pollutants in 31 provincial capital cities based on in situ air quality monitoring data from China National Environmental Monitoring Center, *Environ. Int.*, 86, 92–106, 2016.

Zhao, S. P., Yu, Y., Yin, D., Yu, Z., Dong, L. X., Mao, Z., He, J. J., Yang, J., Li, P., and Qin, D. H.: Concentrations, optical and radiative properties of carbonaceous aerosols over urban Lanzhou, a typical valley city: Results from in-situ observations and numerical model, *Atmos. Environ.*, 213, 470–484, 2019.

Zhao, S. P., Yu, Y., Yin, D. Y., and Qin, D. H.: Contrasting response of ultrafine particle number and  $PM_{2.5}$  mass concentrations to Clean Air Action in China, *Geophys. Res. Lett.*, 48, e2021GL093886, <https://doi.org/10.1029/2021GL093886>, 2021.